JOURNAL OF FOOD PROCESS ENGINEERING

D.R. HELDMAN
and
R.P. SINGH
COEDITORS

FOOD & NUTRITION PRESS, INC.

OLUME 16, NUMBER 2 MAY 1993

JOURNAL OF FOOD PROCESS ENGINEERING

All articles for publication and inquiries regarding publication should be sent to DR. D.R. HELDMAN, COEDITOR, *Journal of Food Process Engineering,* Food Science/Engineering Unit, University of Missouri-Columbia, 235 Agricultural/Engineering Bldg., Columbia, MO 65211 USA; or DR. R.P. SINGH, COEDITOR, *Journal of Food Process Engineering,* University of California, Davis, Department of Agricultural Engineering, Davis, CA 95616 USA.

All subscriptions and inquiries regarding subscriptions should be sent to Food & Nutrition Press, Inc., 2 Corporate Drive, P.O. Box 374, Trumbull, CT 06611 USA.

One volume of four issues will be published annually. The price for Volume 16 is $127.00 which includes postage to U.S., Canada, and Mexico. Subscriptions to other countries are $147.00 per year via surface mail, and $156.00 per year via airmail.

Subscriptions for individuals for their own personal use are $97.00 for Volume 16 which includes postage to U.S., Canada, and Mexico. Personal subscriptions to other countries are $117.00 per year via surface mail, and $126.00 per year via airmail. Subscriptions for individuals should be sent direct to the publisher and marked for personal use.

The *Journal of Food Process Engineering* (ISSN: 0145-8876) is published quarterly (March, June, September and December) by Food & Nutrition Press, Inc.—Office of Publication is 2 Corporate Drive, P.O. Box 374, Trumbull, Connecticut 06611 USA.

Second class postage paid at Bridgeport, CT 06602.

POSTMASTER: Send address changes to Food & Nutrition Press, Inc., 2 Corporate Drive, P.O. Box 374, Trumbull, CT 06611.

JOURNAL OF FOOD PROCESS ENGINEERING

JOURNAL OF FOOD PROCESS ENGINEERING

Journal of FOOD PROCESS ENGINEERING

VOLUME 16
NUMBER 2

Coeditors: D.R. HELDMAN
R.P. SINGH

FOOD & NUTRITION PRESS, INC.
TRUMBULL, CONNECTICUT 06611 USA

ISSN 0145-8876

Printed in the United States of America

CONTENTS

OPTIMAL DESIGN OF A ROTARY CUTTER BY LAGRANGIAN MULTIPLIERS FOR THE CONTINUOUS PRODUCTION OF INDIAN UNLEAVENED FLAT BREAD

B.S. SRIDHAR[1] and B.V. SATHYENDRA RAO[2]

Central Food Technological Research Institute
Mysore 570 013 India

Accepted for Publication August 19, 1992

ABSTRACT

A mathematical approach for the optimal design of a rotary cutter by using Lagrangian Multipliers, in the continuous production of chapatis (Indian unleavened flat bread), is presented.

The objective function has been taken as the output and the constraints have been recognized as diameter and speed of rotation of the roller, number of cutters, diameter of the cutter and gap between the cutters. The numerical profile obtained from the method is in close agreement with the experimental values. It has been observed that, within the range of roller diameters and rotational speeds studied, the roller of diameter 0.165 m with three cutters was optimal with an output of 710 units h^{-1}, leaving about 38% scrap dough for recycling.

INTRODUCTION

Chapati, an unleavened baked product, forms the staple food of large segment of Indian population. With the ever growing demand for ready-to-eat and easy to carry foods, chapatis offer a considerable potential towards mechanization. It is normally made from either whole wheat flour, obtained by grinding in a Plate mill or resultant *atta*, obtained from Roller flour mill. Chapatis are made by kneading flour with water (50–70%) to obtain the dough, which is then rolled into a circular sheet, using a rolling pin. It is then baked on a hot plate on each side for about 1 min at 180–200C and puffed on a live coal or gas (Haridasa

[1]Process Engineering Plant Design Area. The address to which correspondence can be made.
[2]Discipline of Cereal Science and Technology Area.

Journal of Food Process Engineering **16** (1993) 79–92.

Rao and Vatsala 1989). Depending upon the thickness and mode of preparation, chapatis are referred to as tandoori rotis (5–9 mm thickness) and phulkas (1.2–2 mm thickness) (Sidhu and Seibel 1989).

Different approaches towards mechanization of chapatis are in the developmental stages. The production of chapatis is based either on rolling of the dough between one or more pairs of rollers or pressing dough balls between two plates. These systems have many drawbacks like: (1) sticking of the dough between rollers or plates, (2) variation in size and nonuniformity in the thickness of chapatis, (3) reduced output, (4) dough sheet shrinkage and tearing, (5) design restricted to batch production.

To eliminate these problems and to produce uniformly sized chapatis continuously, a rotary cutter was designed. The rarely used Lagrangian Multipliers method was adopted to optimize the Rotary cutter. The theoretical feasibility of using Lagrangian multiplier method for solving certain optimization problems with inequalities, by direct use of external principles has been demonstrated by Pennisi (1953) and Klein (1955). The objective of this paper is to determine the optimality of the rotary cutter for maximum continuous output of chapatis by employing Lagrange's method of undetermined multipliers in its extended form.

The design of the rotary cutter for maximum output depends upon roller diameter, its speed of rotation, gap between the cutters, number and diameter of the cutters. The cutter must be so proportioned that the changes in these parameters do not affect dough sheet output in terms of shrinkage, shearing and space requirement. The number and gap between the cutters decide the extent of dough scrapings for recycling. Therefore, the rotary cutter problem may be formulated as a constrained optimization problem with inequality constraints.

THEORY

The dependent variable to be optimized is the output. The equation for output of the rotary cutter is derived as follows:

Output/min = number of cutters rolled on the dough sheet per minute × revolutions per minute of the roller

$$Q = n \times N \tag{1a}$$

By the geometry of rotary cutter (Fig. 1),

$$\pi D = n\,(c + d) \tag{1b}$$

$$n = \pi\, D/(c + d) \tag{1c}$$

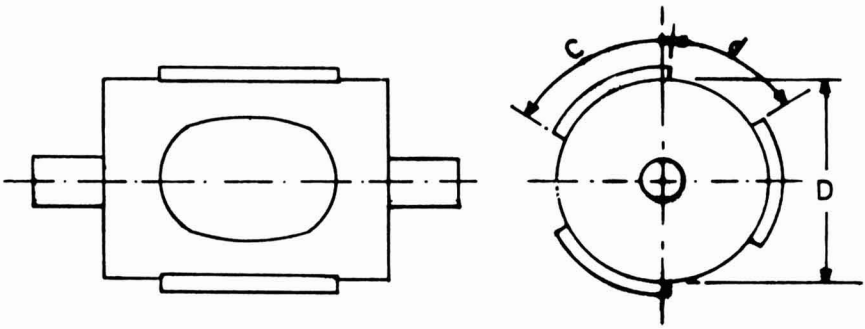

FIG. 1. A ROTARY CUTTER
c = Diameter of the cutter; D = diameter of the roller; d = gap between the cutters.

also $$V = \pi D N \tag{1d}$$

substituting (1b) in (1d), we get

$$V = n (c + d) N \tag{1e}$$

$$N = V/n (c + d) \tag{1f}$$

eqn (1a) becomes

$$Q = \frac{\pi D}{(c + d)} \quad \frac{V}{n (c + d)} \tag{1g}$$

$$Q = \frac{\pi D V}{n (c + d)^2} \tag{1}$$

Thus the constrained design parameters are: diameter of the cutter, equal to the diameter of chapatis (c), number of cutters (n), gap between the cutters (d) and hence the diameter of the roller (D) and speed of rotation of the roller (V).

The method of Lagrangian Multipliers is applied to obtain the optimal output subjected to the above constraints.

The basic equations employed to solve the present problem are in the form:

$$\frac{\partial U}{\partial x_i} + \sum_{j=1}^{m} \lambda_j \frac{\partial}{\partial x_i} (\phi_j + k_j)^2 = 0 \tag{2}$$

$$\frac{\partial U}{\partial x_i} + \sum_{j=1}^{m} \lambda_j \frac{\partial}{\partial k_j} (\phi_j + k_j)^2 = 0 \qquad (3)$$

$$\phi_j + k_j^2 = 0 \qquad (4)$$

where λ_j s are Lagrangian multipliers. The k_j s are introduced as squared quantities to prevent their dropping out after the partial derivatives are taken and to ensure that the slack effect is always positive even though k_j is negative.

These represent (n + 2m) equations in the 'n' unknown x_i s, the 'm' unknown x_i s and k_j s. These simultaneous equations shall be nonlinear. Depending upon the number of variables, the problem can be reduced by an either/or approach.

The theoretical output computation for various rotary cutters, applying the method of Lagragian Multipliers gave an optimal solution: Q = 710 units h^{-1}, V = 2.1 m min^{-1}, C = 0.150 m, d = 0.02279 m, n = 3 and D = 0.165 m. This has been verified experimentally. (Problem example is given in Appendix I).

MATERIALS AND METHODS

All experiments were conducted on an indigenously designed and fabricated equipment for the continuous production of chapatis.

The equipment essentially consists of a tapered screw, a barrel, a fishtail die, a feeder, a rotary cutter and a set of conveyors, (Fig. 2). The rotational speed of the cutter is so synchronized to avoid dough sheet shrinkage and tearing (A patent has been applied for the equipment, covering its several design aspects, Patent Application No. 61/DEL/91, 62/DEL/91 Dt. 23-1-91).

When an elliptical contour is rolled on a horizontal plane, it generates a circle. This principle was adopted in the construction and design of the rotary cutter. The cutter is made of stainless steel grade SS 304 and mounted on a roller of teak wood (Fig. 2).

The production of chapatis, made from wheat flour resultant atta, obtained from Roller flour mill C.F.T.R.I., Mysore (size ~ 150 μm) was used to determine the performance of the rotary cutter. The general steps outlined in Fig. 3, are followed for the production of chapatis. The formation of chapati disc after the dough preparation involves (1) sheeting, (2) cutting and (3) recycling of the trimmings.

Wheat flour was made into dough of desired moisture level (55% w.b.) by spraying water, in a planetary mixer, (Gansons, 50 L). The dough was allowed for about 20 min to assume equilibrium. Sheeting was done from the preconditioned dough by mechanical extrusion and conveyed to a cutting point, where

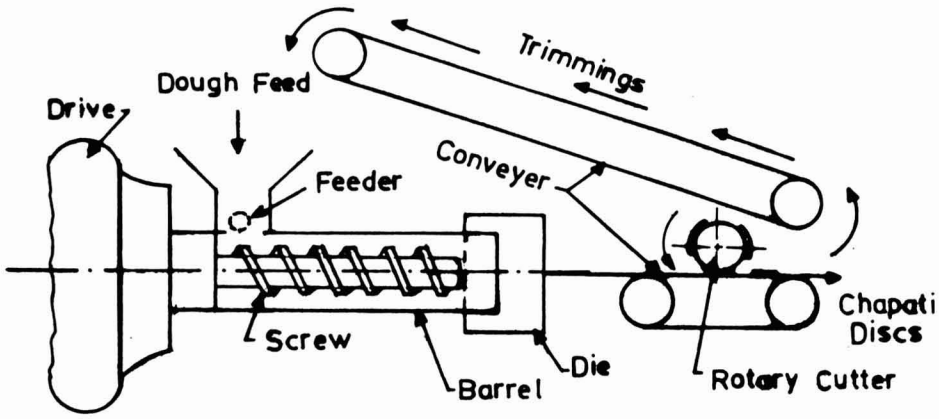

FIG. 2. SCHEMATIC VIEW OF THE EQUIPMENT USED IN CHAPATI PRODUCTION

the rotaray cutter mounted on a stand, rotates in the direction of sheet flow and cuts uniform circular Chapati discs. The trimmings (scrap dough) are conveyed back to the feed point.

This study is a $4 \times 4 \times 3$ factorial design. The ranges of parameters are (a) roller diameter: 0.125, 0.165, 0.185, 0.200 m, (b) rotational speed of the rollers: 0.5, 1.0, 1.5, 2.0 m min^{-1} and (c) number of cutters: 1, 2 and 3.

Trials were conducted under four different sets of conditions to demonstrate the utility of the cutter using the samples of wheat flour with same conditioning. Data were collected after the equipment was allowed to reach steady state. Attainment of steady state was declared when the mechanical energy input variation was less than 1% and Chapatis produced were of uniform size and weight (diameter, thickness and weight of each chapati was 0.150 m, 1.2×10^{-3} and 25×10^{-3} kg, respectively).

RESULTS AND DISCUSSION

The theoretical and experimental changes in output resulting from different speeds of rotation and number of cutters, the relation between the number of cutters and gap between them for different roller diameters are plotted in (Fig. 4 and 5). Table 1 shows the percentage of scrap dough to be recycled at different roller diameters. The theoretical output computation for various roller diameters showed that an output of 710 units h^{-1} and 38% scrap dough was optimal with a configuration of three cutters at a diameter of 0.165 m. These values are in close agreement with the experimental values obtained (700 units h^{-1} production, 38.8 ± 0.7% rejection). The numerical profile variation in the range studied was found to be less than 3%, thus justifying the method adopted.

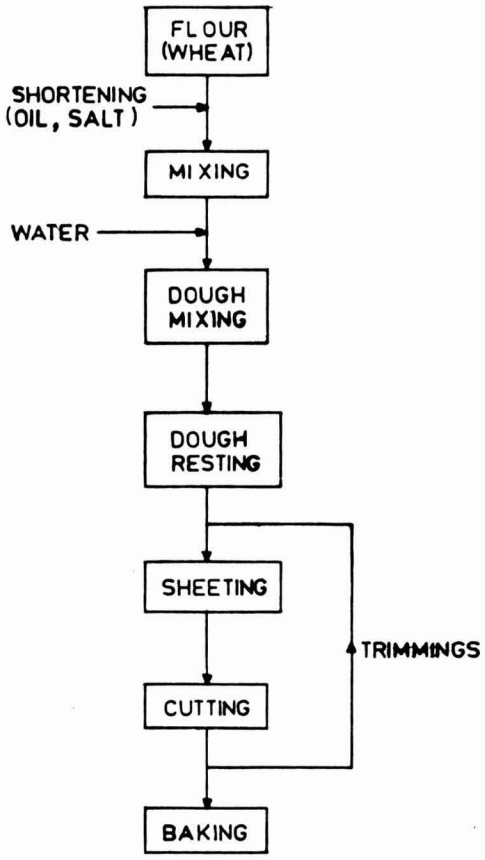

FIG. 3. GENERAL SCHEME FOR THE CONTINUOUS PRODUCTION OF CHAPATIS

The variation in output and scrap dough can be attributed to changes in dough sheet output, variations in moisture content of dough, mechanical energy fluctuations and fabricational error of the cutters.

A decrease in scrap dough/an increase in output occurs when (1) the gap between the cutters is minimum, (2) there is an increase in the number of cutters and (3) there is a reduction in the roller diameter for an increase in circumferential speed. Converse of these cases is also true. (Fig. 4 and 5; Table 1). Also there exists an optimal diameter, for a given number of cutters to achieve the desired optimal output. Cases where the reduction of gap between the cutters increases the production rate cannot be referred to as optimal, because this causes shearing of the dough sheet (small width of trimmings) and related operational (handling) problems, and cases where the number of cutters decreases the per-

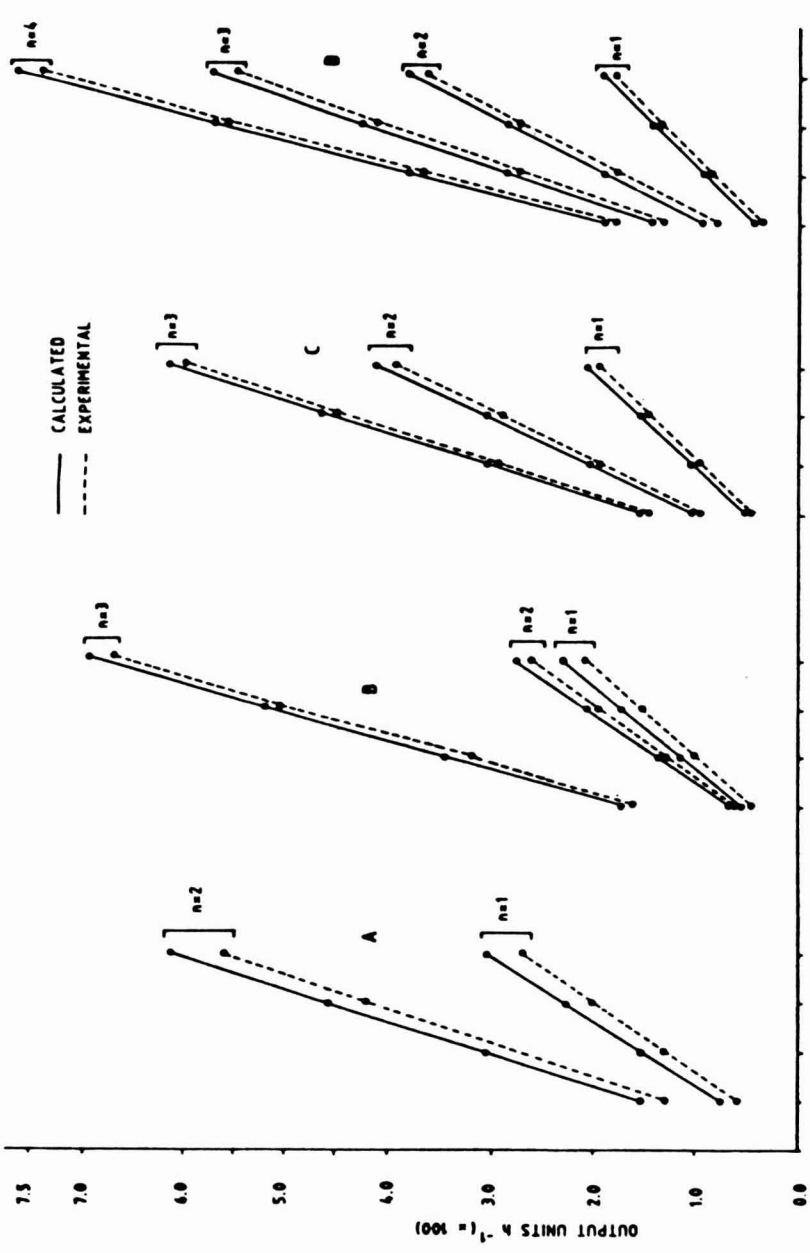

FIG. 4. CHANGES OF OUTPUT AS A FUNCTION OF ROTATIONAL SPEED AT ROLLER DIAMETERS 0.125 (A), 0.165 (B), 0.185 (C), 0.200 (D) m AND NUMBER OF CUTTERS (n = 1 to 4), UNIT WEIGHT OF CHAPATI -25×10^{-3} kg, SIZE: 0.150 m DIA 1.2×10^{-3} THICK. EACH POINT IS A MEAN OF THREE REPLICATES

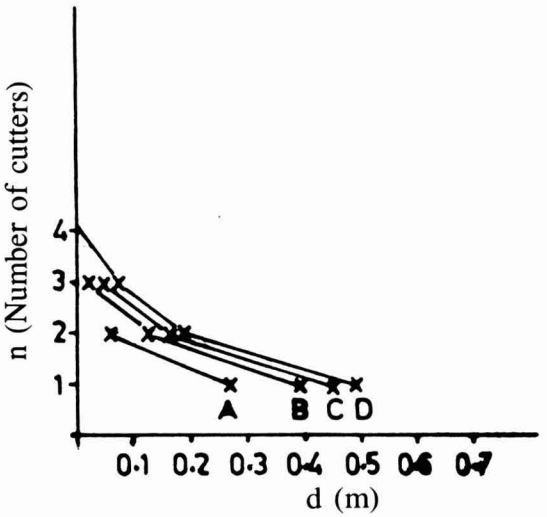

FIG. 5. RELATION BETWEEN NUMBER OF CUTTERS AND GAP BETWEEN THE CUTTERS AT ROLLER DIAMETERS 0.125 (A), 0.165 (B), 0.185 (C), AND 0.200 (D) m. EACH POINT IS A MEAN OF 3 REPLICATES

TABLE 1.
PERCENTAGE SCRAP DOUGH AT VARIOUS ROLLER DIAMETERS AND NUMBER OF CUTTERS*

DIAMETER (m)	NUMBER OF CUTTERS			
	1	2	3	4
0.125	74.5 ± 1.8	48.9 ± 3.4	—	—
0.165	80.2 ± 0.9	61.8 ± 3.1	38.8 ± 0.7	—
0.185	82.2 ± 0.7	66.5 ± 3.4	45.4 ± 0.6	—
0.200	83.3 ± 0.4	68.5 ± 2.6	51.3 ± 2.4	33.1 ± 1.3

*Data are averages of 3 determinants listed as mean ± confidence interval with a confidence coefficient of 98%.

cent scrap dough are not to considered optimal for there is 30% increase in overall space requirements, for every additional cutter. (Present study has been restricted to a circumferential speed of 2.1 m min^{-1} of the roller).

The general expression relating the percentage scrap dough to diameter in 'm's is:

$$P(D) = A_0D^3 + A_1D^2 + A_2D + A_3 \quad (5)$$

where P (D) is the percentage scrap dough, and 'D' is the diameter of the roller, A_0, A_1, A_2 and A_3 are functions of 'n' the number of cutters (Table 2). On comparing the values of output, percentage scrap dough and gap between the cutters of various roller diameters (Fig. 4 and 5; Table 1) and space requirement, a roller with three cutters, and diameter of 0.165 m with three cutters has been chosen as the optimal cutter.

CONCLUSIONS

A mathematical approach for the optimal design of a rotary cutter to maximize output using an extension of Lagrange's multiplier method by adding slack variables when the constraints are of the inequality type has been described. Within the range of roller diameters (0.125–0.200 m) and speed of rotation (1–2 m min^{-1}, the optimal conditions were considered to be 0.165 m diameter roller with three cutters giving a maximum output of 710 units h^{-1} and about 38% scrap dough. The results obtained are in a relatively good agreement with the experimental data. The method can be (1) sufficiently useful in optimizing individual processes under multivariate conditions and scale up, (2) applied to composite systems comprising of multivariate subsystems and (3) used to predict the optimal processing and machine variables.

TABLE 2.
REGRESSION VALUES OF CONSTANTS IN THE EQUATION
$P(D)^* = A_0D^3 + A_1D^2 + A_2D + A_3$

n	A_0	A_1	A_2	A_3
1	5.7461×10^3	-3.648×10^3	8.576×10^2	0.1124×10^2
2	-2.3491×10^4	9.825×10^3	-1.0391×10^3	0.7125×10^2
3	8.2531×10^4	-4.9898×10^4	10.201×10^3	-6.567×10^2
4	3.602×10^5	-1.7108×10^5	2.6751×10^4	-1.374×10^3

*P(D) is the percentage scrap dough; D = Diam of the Roller.

NOMENCLATURE

c Diameter of cutter, m
d Gap between cutters, m
D Diameter of roller, m
k_j Slack variables
N Speed of roller, rev min^{-1}
n Number of cutters
P Scrap dough, percent
Q Output, units h^{-1}
U Objective function
V Circumferential speed of the roller m min^{-1}
x_i Independent design variables
$\emptyset_j$ Inequality constraints

APPENDIX I

The objective function U = MAXIMIZING OUTPUT, Q
The optimization problem:

$$\text{MAXIMIZE } Q = Q(D,V)$$

Subject to:

Roller diameter	$D \leqslant 0.165$ m
Speed of rotation	$V \leqslant 2.1$ m min^{-1}
Gap between cutters	$d \leqslant 0.025$ m
Number of cutters	$n \leqslant 3$
Cutter diameter	$c = 0.150$ m (6)

Solution to the problem:

Substituting the values of constraints in Eq. (1) the optimization equation for output becomes,

$$Q = \frac{\pi D V}{n (0.15 + d)^2} = \text{maximum} \quad (7)$$

The limit equations are:

$$V - 2.10 \leq 0 \quad (8)$$

$$n (0.15 + d) - 0.165 \leq 0 \quad (9)$$

$$n - 3 \leq 0 \qquad \text{where n is a +ve whole number} \tag{10}$$

$$d - 0.025 \leq 0 \tag{11}$$

Introducing slack variables

$$V - 2.10 + + k_1^2 = 0 \tag{12}$$

$$\frac{n}{\pi}(0.15 + d) - 0.165 + k_2^2 = 0 \tag{13}$$

$$n - 3 + k_3^2 = 0 \tag{14}$$

$$d - 0.025 + k_4^2 = 0 \tag{15}$$

Applying Eq. (2) to (4) to Eq. (7), (12), (13), (14) and (15),

$$\frac{\partial}{\partial V}\left[\frac{\pi D V}{n (0.15 + d)^2}\right] + \lambda_1 \frac{\partial}{\partial V}[V - 2.10 + k_1^2] +$$

$$\lambda_2 \frac{\partial}{\partial V}[n (0.15 + d) - 0.165 + k_2^2] + \lambda_3 \frac{\partial}{\partial V}[n - 0.3 + k_3^2] +$$

$$\lambda_4 \frac{\partial}{\partial V}[d - 0.025 + k_4^2] = 0 \tag{16}$$

$$\frac{\pi D}{n (0.15 + d)^2} + \lambda_1 + 0\lambda_2 + 0\lambda_3 + 0\lambda_4 = 0 \tag{17}$$

Similarly after performing partial differentiation with respect to 'n', 'd' and the variable 'k_j's, we get,

$$\frac{-\pi D V}{n^2 (0.15 + d)^2} + 0\lambda_1 + (0.15+d)\lambda_2 + \lambda_3 + 0\lambda_4 = 0 \tag{18}$$

$$\frac{-2\pi D V}{n (0.15 + d)^3} + 0\lambda_1 + n\lambda_2 + 0\lambda_3 + \lambda_4 = 0 \tag{19}$$

$$2\lambda_1 K_1 = 0 \tag{20}$$

$$2\lambda_2 K_2 = 0 \tag{21}$$

$$2\lambda_3 K_3 = 0 \tag{22}$$

$$2\lambda_4 K_4 = 0 \tag{23}$$

In addition to these equations, Eq. (12) to (15) must also be solved simultaneously.

Now this problem is solved by logical either/or approach (elimination method). The possible solutions for λs are presented in Table 3.

Elimination of solutions is based on the criteria:

Solution 1. Case where $\lambda_1 = 0$ Eq. (17) and
$\lambda_2 = 0$, $\lambda_3 = 0$, and $\lambda_4 = 0$ Eq. (18) and (19)
2. Case where $\lambda_2 = \lambda_3 = \lambda_4 = 0$ Eq. (18) and (19)

TABLE 3.
POSSIBLE SOLUTION FOR λ

Solution No.	λ_1	λ_2	λ_3	λ_4	Possible Solution	Remarks
1	0	0	0	0	No	N.F
2.	-	0	0	0	No	N.F
3.	0	-	0	0	No	N.F
4.	0	0	-	0	No	N.F
5.	0	0	0	-	No	N.F
6.	-	-	0	0	Yes	Feasible Solution
7.	0	-	-	0	No	N.F
8.	0	0	-	-	No	N.F
9.	-	0	0	-	No	N.F
10.	0	-	0	-	No	N.F
11.	-	0	-	0	No	N.F
12.	-	-	-	0	Yes	Feasible Solution
13.	-	-	0	-	Yes	Feasible Solution
14.	-	0	-	-	Yes	Feasible Solution
15.	0	-	-	-	No	N.F
16.	-	-	-	-	-	Unbound

N.F. = Not Feasible.

3. Case where $\lambda_1 = \lambda_3 = \lambda_4 = 0$	Eq. (17)
4. Case where $\lambda_1 = \lambda_2 = \lambda_4 = 0$	Eq. (17) and (19)
5. Case where $\lambda_1 = \lambda_2 = \lambda_3 = 0$	Eq. (17) and (18)
6. Feasible solution $\lambda_3 = \lambda_4 = 0$ and $k_1 = 0, k_2 = 0$	
7. Case where $\lambda_1 = \lambda_4 = 0$	Eq. (17)
8. Case where $\lambda_1 = \lambda_2 = 0$	Eq. (17)
9. Case where $\lambda_2 = \lambda_3 = 0$	Eq. (18)
10. Case where $\lambda_1 = \lambda_3 = 0$	Eq. (17)
11. Case where $\lambda_2 = \lambda_4 = 0$	Eq. (19)
12. Feasible solution: $\lambda_4 = 0$; $k_1 = k_2 = k_3 = 0$	
13. Feasible solution: $\lambda_3 = 0$; $k_1 = k_2 = k_4 = 0$	
14. Feasible solution: $\lambda_2 = 0$; $k_1 = k_3 = k_4 = 0$	
15. Case where $\lambda_1 = 0$	Eq. (17)
16. Case where $\lambda_1 = \lambda_2 = \lambda_3 = \lambda_4 = 0$	– UNBOUND

The feasible solutions (6), (12), (13) and (14) are now examined:

Solution (6):

$\lambda_3 = 0$, $\lambda_4 = 0$; $k_1 = 0$; $k_2 = 0$

$V = 2.10$ by Eq. (12)

$\frac{n}{\pi}(0.15 + d) = 0.165$ by Eq. (13)

hence, $d = (0.165\ \pi/n) - 0.15$

and thus the solution is INCOMPLETE. — NOT FEASIBLE

Solution (12):

$\lambda_4 = 0$; $k_1 = k_2 = k_3 = 0$

$V = 2.10$ by Eq. (12)

$\frac{n}{\pi}(0.15 + d) = 0.165$ by Eq. (13)

$n = 3$ by Eq. (14)

$d = 0.02279$, by substituting values in Eq. (15)

— FEASIBLE SOLUTION

Solution (13):

$\lambda_3 = 0$; $k_1 = k_2 = k_4 = 0$

$V = 2.10$ by Eq. (12)

$\frac{n}{\pi}(0.15 + d) = 0.165$ by Eq. (13)

$d = 0.025$ by Eq. (15)
$n = 2.962$, not a whole number
— NONFEASIBLE SOLUTION

Solution (14):
$\lambda_2 = 0$; $k_1 = k_3 = k_4 = 0$
$V = 2.10$ by Eq. (12)
$n = 3$ by Eq. (14)
$d = 0.025$ by Eq. (15)
$k_2^2 = -ve$, substituting values in Eq. (13)
— NONFEASIBLE SOLUTION

Therefore the possible solution (12) is the only solution and is the optimal solution.

The optimal solution gives $D = 0.165$ m, $V = 2.1$ m min^{-1}, $c = 0.150$ m, $d = 0.02279$ m, $n = 3$ and $Q = 710$ units h^{-1}.

REFERENCES

HARIDASA RAO, P. and VATSALA. 1989. Effect of damaged starch on the chapati making quality of whole wheat flour. Cereal Chem. *65*, 157.

KLEIN, B. 1955. Direct use of External principles in solving certain optimization problems involving inequalities. Operation Res. *2*, 168–169.

PENNISI, L.L. 1953. An introduction to sufficiency proof for the problem of Lagrange with differential inequalities as Added side constraints. Amer. Math. Soc. Trans. *74*, 171–174.

SIDHU and SEIBEL. 1989. Effect of shortening on chapati quality. Cereal Food World, p. 286–289.

ANALYSIS OF THE HELICAL SCREW RHEOMETER FOR FLUID FOOD

MAGDALENA S. TAMURA[1]

Department of Agricultural Engineering
University of California, Davis

JERALD M. HENDERSON[2]

Departments of Mechanical Engineering and Food Science & Technology
University of California, Davis

ROBERT L. POWELL

Department of Chemical Engineering
University of California, Davis

CHARLES F. SHOEMAKER

Department of Food Science & Technology
University of California, Davis

Accepted for Publication December 1, 1992

ABSTRACT

The Helical Screw Rheometer (HSR) is being evaluated for rheological measurements of fluid food suspensions. The HSR consists of a helical screw enclosed in a tight fitting cylinder. With a closed system the inner screw is rotated creating a linearly increasing pressure differential along the axis of the screw, which is proportional to the viscosity of the fluid. This paper presents theoretical one- and two-dimensional flow analyses for Newtonian fluids using both rectangular and cylindrical coordinates. For non-Newtonian fluids a one-dimensional rectangular analysis was developed using the power law model.

[1]Current address: Ares-Serono, 15 BIS, Chemin Des Mines CH1211, Geneva, Switzerland.
[2]Correspondence: J.M. Henderson, Mechanical Engineering, University of California, Davis, CA 95616.

Journal of Food Process Engineering **16** (1993) 93–126.

INTRODUCTION

During food processing marked physical and chemical changes can occur, so it is desirable to monitor the process to achieve greater process and quality control (Rao 1977a). On-line rheological measurements in the food industry have been limited (Whorlow 1980; Van Wazer *et al.* 1963; Tily 1983) and the available instruments do not measure fundamental physical parameters; they are primarily empirical in nature. Viscosity, the measure of a fluid's resistance to flow or change in shape, is one of many rheological parameters and is indicative of the physical and chemical composition of the fluid.

Newtonian fluids are characterized by a linear relationship between shear stress and shear rate where

$$\tau = \mu \dot{\gamma} \tag{1}$$

τ is the shear stress (dynes/cm^2), $\dot{\gamma}$ is the shear rate (s^{-1}), and μ is the viscosity. The traditional units for μ are poise (dynes-s/cm^2) and the standard SI unit is Pa·s (N·s/m^2) where 10 poise = 1 Pa·s. This single coefficient μ sufficiently characterizes an incompressible Newtonian fluid. It depends on temperature and pressure only, and it is independent of shear rate and time of shearing.

Most fluid food products do not follow the Newtonian rheological model. For many common foods the shear stress is dependent on the shear rate; hence, a nonlinear relationship results and a unique viscosity constant is no longer adequate to characterize the fluid. However, it is common practice to use the ratio of shear stress to shear rate as the "apparent viscosity" for non-Newtonian fluids.

A single constant is not sufficient to characterize the shear stress versus shear rate behavior of a non-Newtonian fluid. A common non-Newtonian model used for this purpose is the power law model (Rao 1977b) defined as

$$\tau = m\dot{\gamma}^n \tag{2}$$

The consistency index, m, is generally an indication of solids content and is relatively sensitive to temperature (Holdsworth 1971). The power law index, n, is dimensionless and ranges between 0 and 1 for most fluid foods. The Newtonian case is obtained when n = 1 and m = μ. The value of n decreases with increasing molecular weight, and sometimes, solids content. The power law index is a direct indicator of the departure from Newtonian flow. The apparent viscosity for a power law fluid is obtained by dividing the shear stress by shear rate,

$$\mu_a = m\dot{\gamma}^{n-1} \tag{3}$$

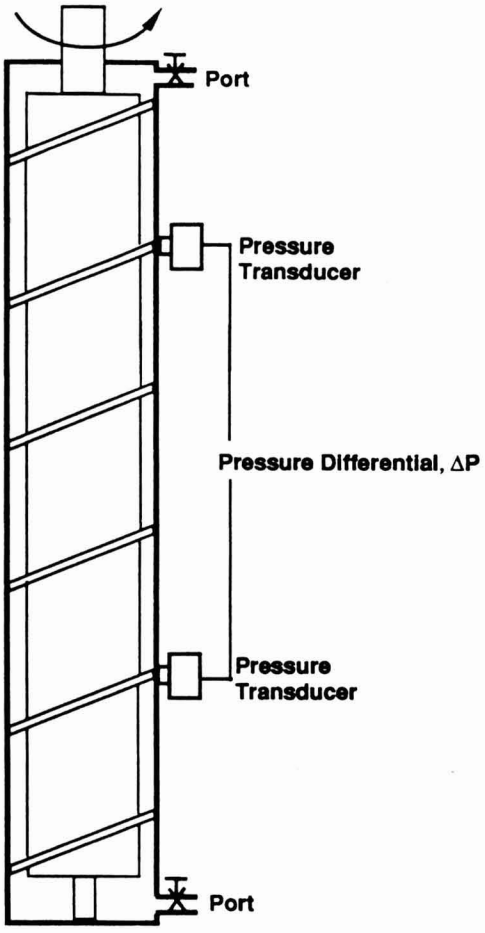

FIG. 1. SCHEMATIC DIAGRAM OF THE
HELICAL SCREW RHEOMETER (HSR)

Fluid viscosity measurements with most current viscometers used in processing systems are obtained by empirically correlating a measured quantity with an apparent viscosity. Hence, the objective of a recent study was to study an alternative instrument that could characterize fluid food accurately and consistently (Tamura 1989). A review of the literature and the U.S. patents did not elicit any applicable methods for food suspensions, except for the Helical Screw Rheometer (HSR), which was recently revived by Kraynik *et al.* (1984a, b) for use in coal

liquefaction processing. The work reported here is based on Kraynik's work and the goal of this paper is to clarify and extend that work.

The HSR consists of a helical screw enclosed in a tight fitting cylinder as shown in Fig. 1. With the inlet and outlet ports closed the inner screw is rotated at a constant angular speed creating a pressure differential along the axis of the screw. This pressure differential increases linearly along the axis of the screw and is proportional to the viscosity of the fluid. This paper develops the theoretical flow analysis for Newtonian fluids and power law fluids in the HSR.

PROBLEM DEFINITION

The HSR geometry is shown in Fig. 2. To understand the geometrical parameters it is helpful to "unwrap" the helical channel. As suggested by Tad-

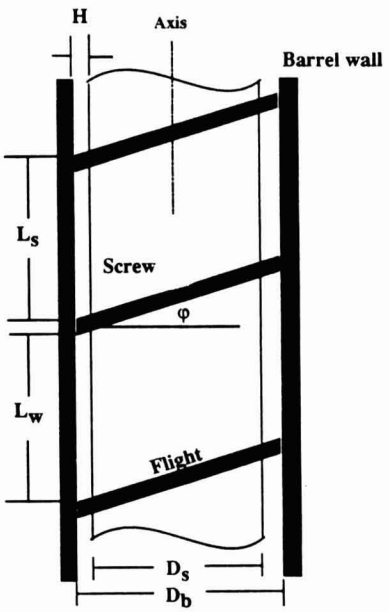

FIG. 2. GEOMETRICAL PARAMETERS OF THE HSR

D_s = minor diameter or screw root diameter; D_b = major diameter or inner barrel diameter; φ = flight angle or helix angle at the barrel surface; L_s = flight lead; L_w = distance between flights; H = radial distance between screw root and barrel diameter.

mor and Klein (1970), it is easy to visualize the "unwrapping" of the screw by rotating the screw, with ink-painted flights, on a piece of paper. The trace left on the paper would be the "unwrapped" channels. But the screw is one continuous channel and can be thought of as forming a shallow rectangular channel as shown in Fig. 3. The "flattened" barrel forms the flat plate over the channel.

A complete flow analysis of the fluid in the HSR is necessary to determine the relationships between the measured parameters — pressure differential (ΔP) and rotational rate (N), to the Newtonian viscosity or to the non-Newtonian power-law parameters. Since the geometry of a HSR is similar to a single-screw extruder, much of the analysis developed follows classical extrusion theory (McKelvey 1962; Tadmor and Klein 1970; Tadmor and Gogos 1979; Rauwendaal 1986).

In the flow analysis there are two simplifying approaches that can be taken. In the first approach, the effect of curvature is neglected. As previously described the helical channel is "unwrapped", and the geometry is approximated as a rectangular channel confined by a flat plate (Fig. 3). A on-dimensional rectangular analysis is performed, and then a more general two-dimensional rectangular analysis is discussed. The second approach takes into account the curvature by using cylindrical coordinates. In all cases, however, some common assumptions are made.

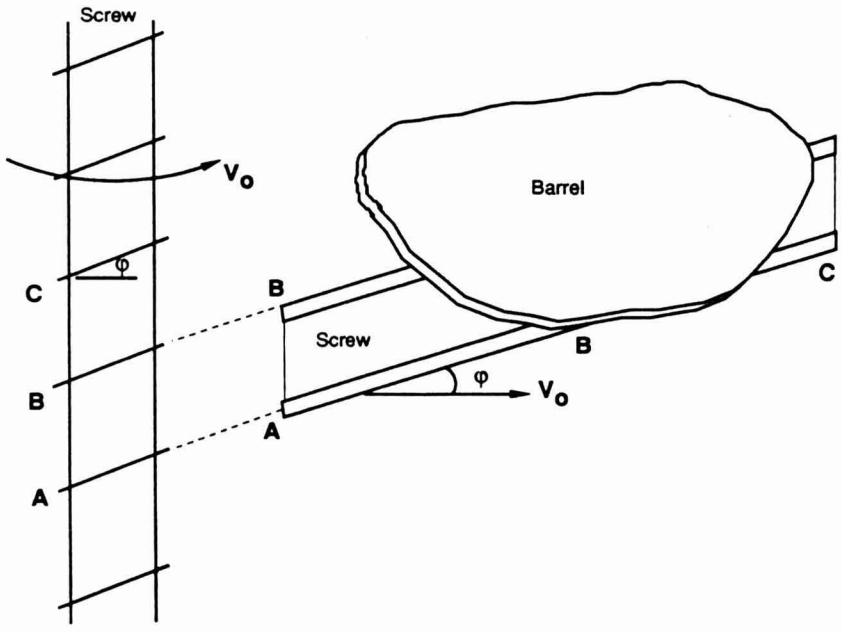

FIG. 3. THE UNWRAPPED HELICAL CHANNEL AS A SHALLOW RECTANGULAR CHANNEL BOUND BY A FLAT BARREL PLATE

(1) The flow is in steady state.
(2) The flow is laminar.
(3) No slippage of the fluid occurs at the surface of the rotating screw or at the barrel.
(4) No leakage of the fluid occurs across the flights.
(5) The flow is isothermal; viscous heating effects are negligible.
(6) The effect of gravity is neglected.
(7) A shallow channel is assumed where the channel width, W, is considered much greater than the gap, H, ($H/W << 1$).
(8) The fluid is incompressible.
(9) All screw and barrel surfaces are wetted by the fluid.
(10) Deviations in flow at the ends of the screw are neglected.

The fundamental governing equations are equations of continuity and momentum, in addition to constitutive equations (Bird *et al.* 1960).

The continuity equation or conservation of mass is

$$\frac{D\rho}{Dt} = -\rho\,(\nabla\cdot\mathbf{v}) \tag{4}$$

where ρ is the fluid density, $\mathbf{v}$ the velocity vector, t is time and D/dt is the material derivative and Δ is the gradient operator. Since the fluid is assumed incompressible, $\frac{D\rho}{Dt} = 0$. Equation (4) simplifies to

$$0 = \nabla\cdot\,\mathbf{v} \tag{5}$$

In rectangular coordinates the simplified equation is of the form

$$\frac{d(v_x)}{dx} + \frac{d(v_y)}{dy} + \frac{d(v_z)}{dz} = 0 \tag{6}$$

and in cylindrical coordinates

$$\frac{1}{r}\frac{d}{dr}(v_r) + \frac{1}{r}\frac{d}{d\theta}(v_\theta) + \frac{d}{dz}(v_z) = 0. \tag{7}$$

The conservation of linear momentum, also referred to as the equation of motion, results from Newton's second law where the relevant forces are due to pressure, viscosity, and gravity, or

$$\rho \frac{D\mathbf{v}}{Dt} = -\nabla \mathbf{P} - [\nabla \cdot \tau] + \rho \mathbf{g} \tag{8}$$

where **P** is the pressure, **g** is the gravitational acceleration, and τ is the viscous stress tensor. This results in three unknowns **v**, τ and **P**. Therefore, constitutive equations relating the stress tensor to the rate of deformation tensor are necessary to obtain a complete solution. The solution to these equations yields the velocity distribution, flow rate, and the shear rate and shear stress relationships.

The stress tensor describes the forces acting between neighboring elements in a fluid (Tadmor and Klein 1970). There are six independent components, three of them being normal stresses. For a Newtonian fluid the constitutive equation is $\nabla \cdot \tau = \mu \nabla^2 \mathbf{v}$. When this shear stress tensor is combined with Eq. (8) we obtain the Navier-Stokes equations where

$$\rho \frac{D\mathbf{v}}{Dt} = -\nabla \mathbf{P} + \mu \nabla^2 \mathbf{v} + \rho \mathbf{g}. \tag{9}$$

NEWTONIAN ONE-DIMENSIONAL RECTILINEAR FLOW ANALYSIS

In the rectilinear flow analysis of the HSR the effect of curvature is neglected where the helical channel is approximated as a rectangular channel when the channel is assumed unwrapped from the screw as shown in Fig. 4a (Pearson 1985; Tadmor and Gogos 1979). The rectangular coordinates are positioned so that x is the axial direction and z coincides with the direction of the screw rotation.

The flow is assumed to occur in the x-z plane only, hence, $v_y = 0$ and $dv_y/dy = 0$. If a fully developed flow is assumed (except near the flights) then $v_x \neq v_x(x)$ and $v_z \neq v_z(z)$ and the continuity equation (Eq. 6) would hold because $dv_x/dx = 0$ and $dv_z/dz = 0$.

$$\cancel{\frac{dv_x}{dx}}^{\,0} + \cancel{\frac{dv_y}{dy}}^{\,0} + \frac{dv_z}{dz} = 0 \tag{10}$$

Since at the ends of the screw channel v_x is zero (closed discharge) and v_x is constant along x($v_x \neq v_x(x)$), then, v_x must be zero everywhere (Fig. 4a). This also implies that $\partial P/\partial x = 0$; hence, there are isobars in the x-direction. The dominant flow is in the z-direction except for circulation near the flights, which is considered negligible for a narrow gap relative to the width of the channel. The

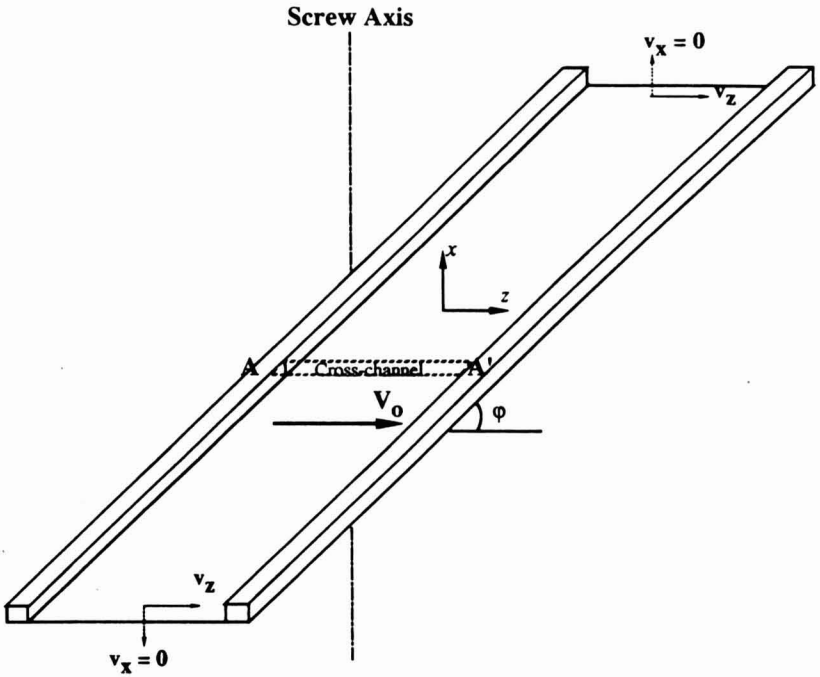

FIG. 4a. HELICAL CHANNEL APPROXIMATED AS A RECTANGULAR CHANNEL
The x- and z- directions are on the plane of the paper and y-direction is normal to the paper. Flow in the HSR is in the direction of rotation, V_o, so the one-dimensional analysis focuses on the cross-channel A to A′.

fluid then flows only in the direction of the barrel rotation (z-direction) or from A to A′ as shown in Fig. 4a. The cross-sectional view of A to A′ is shown in Fig. 4b, which illustrates the actual channel where flow occurs. The flow analysis, initially focuses across this cross-channel, rather than the total unwrapped helical channel. The problem is, thus, considered one-dimensional where mathematically, the flow is dependent on only one variable, y.

The velocity profile is first obtained by simplifying the relevant equations of motion. As determined above, there is only one velocity component, $v_z = v_z(y)$ so the relevant stresses are a function of y only ($\frac{\partial \tau_{yx}}{\partial y}$, $\frac{\partial \tau_{yy}}{\partial y}$ and $\frac{\partial \tau_{yz}}{\partial y}$). But for laminar flow the only stress acting between the fluid layers is τ_{yz} (Fig. 4c) and Eq. (8) reduces in the absence of gravity to

$$0 = -\frac{\partial P}{\partial z} - \frac{\partial \tau_{yz}}{\partial y} \qquad \text{(y-component)} \qquad (11)$$

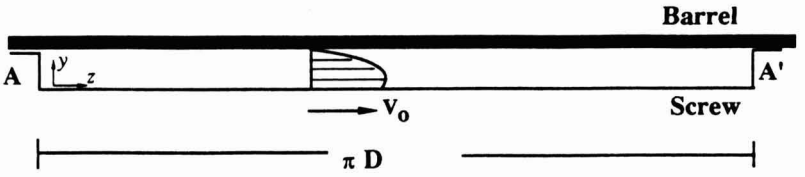

FIG. 4b. CROSS-CHANNEL FROM AN UNWRAPPED HELICAL CHANNEL
The length of the channel corresponds to the circumference of the barrel.

By substituting the Newtonian constitutive equations

$$\tau_{yz} = -\mu \frac{dv_z}{dy} \tag{12}$$

Eq. (11) becomes

$$\frac{\partial P}{\partial z} = \frac{\partial^2 v_z}{\partial y^2} \mu. \tag{13}$$

Since the left side of the equation is a function of z only, while the right side is a function of y only, the equation becomes an ordinary differential equation. By integrating twice the velocity profile obtained is

$$v_z = \frac{1}{2\mu} \frac{dP}{dz} y^2 + C_1 y + C_2 \tag{14}$$

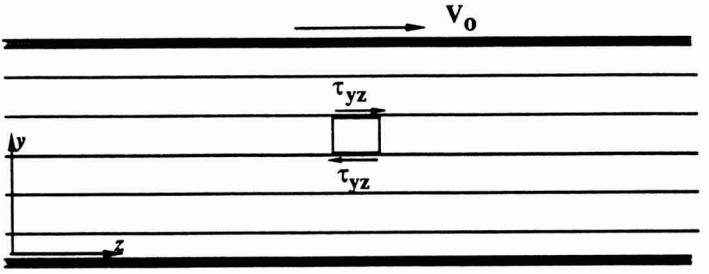

FIG. 4c. A FLUID ELEMENT SHEARED IN LAMINAR FLOW EXPERIENCES STRESSES IN EQUAL AND OPPOSITE DIRECTIONS

The constants of integration C_1 and C_2 are evaluated with the following boundary conditions. At the screw root where $y = 0$ the fluid velocity $v_z = 0$, and at the barrel surface, where $y = H$, the fluid velocity moves at the velocity of the rotating barrel, $v_z = V_o$. Therefore, the final velocity profile is

$$v_z = \frac{V_o}{H} y + \frac{1}{2\mu} \frac{dP}{dz} [y^2 - Hy]. \tag{15}$$

The first term on the right side of Eq. (15) is considered to be the drag flow velocity and the second term the pressure flow velocity. In Fig. 5a and 5b these two velocity profiles are shown. The drag flow velocity profile is linear, which would result if the plates are considered infinite and unbounded, whereas the pressure flow velocity profile is parabolic due to the pressure gradient caused by the presence of the screw flights. The combination of these two profiles yields the profiles given in Fig. 5c. The actual profile obtained depends on the direction of the pressure gradient.

To obtain the flow rate profile, it is convenient to first nondimensionalize the velocity profile by letting

$$u_z = \frac{v_z}{V_o} \tag{16}$$

and

$$\xi = \frac{y}{H} \tag{17}$$

to obtain the dimensionless form of the velocity profile [Eq.(15)] as

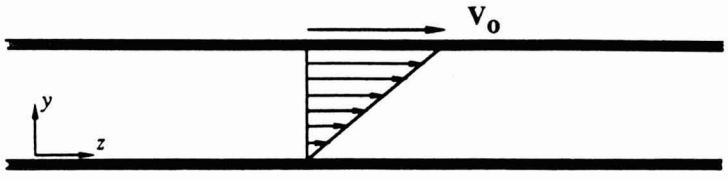

FIG. 5a. DRAG FLOW BETWEEN A MOVING AND STATIONARY PLATE RESULTS IN A LINEAR VELOCITY PROFILE

$$u_z = \xi - 3\xi(1-\xi)\left[\frac{H^2}{6\mu V_o}\frac{dP}{dz}\right] \tag{18}$$

The flow rate per unit width, obtained by integrating the velocity profile across the gap is

$$\frac{Q}{HV_o} = \int_0^1 u_z \, d\xi \tag{19}$$

whereupon substitution of Eq. (18) and subsequent integration results in

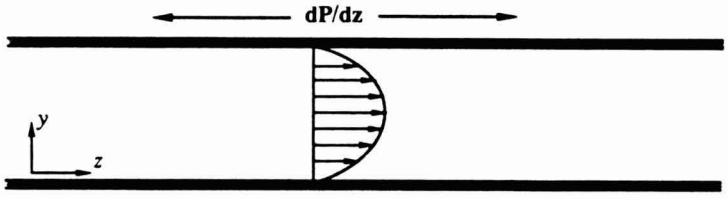

FIG. 5b. PRESSURE FLOW, AS IN A PIPE, RESULTS IN A PARABOLIC PROFILE

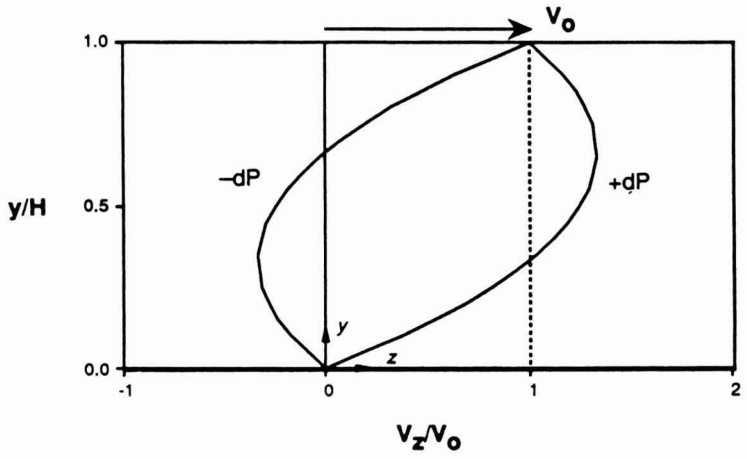

FIG. 5c. TWO VELOCITY PROFILES BETWEEN PARALLEL PLATES FROM A COMBINATION OF DRAG AND PRESSURE FLOW WITH POSITIVE AND NEGATIVE PRESSURE GRADIENTS

$$Q = \frac{V_o H}{2} + \frac{H^3}{12\mu}\left[-\frac{dP}{dz}\right]. \tag{20}$$

The flow rate, as was the velocity, is also considered to consist of two components — the drag flow rate and pressure flow rate, defined as

$$Q_D = \frac{V_o H}{2} \tag{21}$$

$$Q_P = \frac{H^3}{12\mu}\left[-\frac{dP}{dz}\right] \tag{22}$$

respectively, such that Eq. (20) can now be rewritten as

$$Q = Q_D + Q_P \tag{23}$$

If a dimensionless flow rate is defined as the ratio between these flow rate components as

$$\frac{Q_P}{Q_D} = \frac{Q - Q_D}{Q_D} \tag{24}$$

then substitution of Eq. (21) and (22) yields

$$\frac{Q_P}{Q_D} = \frac{H^2}{6\mu V_o}\left[-\frac{dP}{dz}\right]. \tag{25}$$

The velocity profile in Eq. (18) can now be rewritten in terms of this ratio [Eq. (25)] as follows

$$u_z = \xi - 3\xi(1-\xi)\left[-\frac{Q_P}{Q_D}\right]. \tag{26}$$

The velocity in this form is very useful. First, consider the case where the flow is between two parallel plates (without the channel walls). The flow would be

solely due to drag from the moving plate so that $Q_p = 0$ and, therefore, $Q_p/Q_D = 0$. Equation (26), then, reduces to

$$u_z = \xi \tag{27}$$

which is the linear velocity profile shown in Fig. 5a. However, if the channel walls are present the velocity profile is no longer linear. By confining the flow between the channel walls there is no net flow rate ($Q = 0$), thus creating a pressure gradient. The flow rate ratio, $Q_P/Q_D = -1$, and the velocity becomes

$$u_z = \xi - 3\xi(1-\xi)[+1] \tag{28}$$

where the resulting velocity profile (Fig. 6a) now consists of two layers of fluid flowing in opposite directions. The fluid circulates by turning at the flights or channel walls as shown in Fig. 6b.

The shear rate is determined from

$$\dot{\gamma} = \frac{dv_z}{dy} = \left(\frac{dv_z}{d\xi}\right)\left(\frac{d\xi}{dy}\right) \tag{29}$$

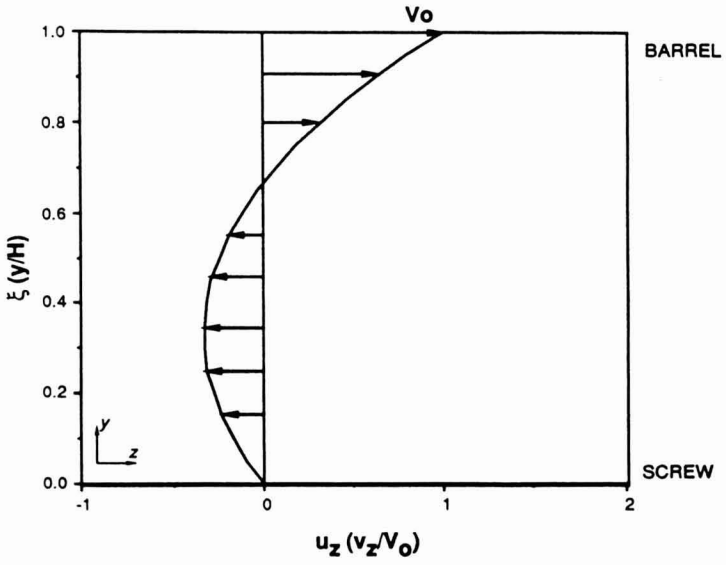

FIG. 6a. VELOCITY PROFILE WITH A ROTATING BARREL AND A STATIONARY SCREW ($Q_P/Q_D = -1$)

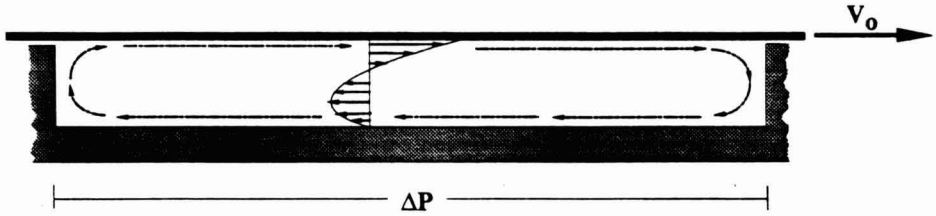

FIG. 6b. TWO LAYERS OF FLUID FLOWING IN OPPOSITE DIRECTIONS IN THE CHANNEL DUE TO PRESSURE AND DRAG FLOW
The fluid circulated by turning at the flights or channel walls.

where

$$\frac{d\xi}{dy} = \frac{1}{H} \tag{30}$$

If the barrel rotates (from Eq. 16 and 28),

$$v_z = V_o [\xi - 3\xi(1-\xi)] \tag{31}$$

then,

$$\frac{dv_z}{dx} = V_o [1-3 + 6\xi] \tag{32}$$

so the shear rate is

$$\dot{\gamma} = \frac{V_o}{H} [6\xi-2] \tag{33}$$

Therefore, at the screw surface $\dot{\gamma} = -2V_o/H$ and at the barrel surface $\dot{\gamma} = 4V_o/H$.

This indicates that the shear rate depends on the position along the gap, and that the fluid next to the dragging surface is subjected to twice the shear of the fluid next to the stationary surface. Since in the previous analysis the barrel was assumed to rotate, when in reality the screw rotates in the HSR case, the above analysis must be reconsidered.

When the screw is rotated, instead of the barrel, the entire channel moves while the plate remains stationary (Fig. 4b). As the channel moves at velocity V_o, past

the observer on the stationary plate, there is an apparent net flow rate per unit width of $Q = V_oH$ where Eq. (20) now becomes

$$V_oH = \frac{V_oH}{2} + \frac{H^3}{12\mu}\left[-\frac{dP}{dz}\right] \tag{34}$$

Simplifying

$$0 = -\frac{V_oH}{2} + \frac{H^3}{12\mu}\left[-\frac{dP}{dz}\right] \tag{35}$$

By using the $Q = Q_D + Q_P$ relationship, the drag flow rate differs from Eq. (21) in sign,

$$Q_D = -\frac{V_oH}{2} \tag{36}$$

and consequently the dimensionless flow rate also changes sign to

$$\frac{Q_P}{Q_D} = +\frac{H^2}{6\mu V_o}\left[\frac{dP}{dz}\right]. \tag{37}$$

Applying the zero net flow rate condition within the channel, the Q_P/Q_D ratio remains -1, but the dimensionless velocity becomes

$$u_z = \xi - 3\xi(1-\xi)\left[+\frac{Q_P}{Q_D}\right] \tag{38}$$

and, hence,

$$u_z = \xi - 3\xi(1-\xi)\,[-1] \tag{39}$$

which is a different velocity profile (Fig. 7). Since the two velocity profiles in Fig. 6a and Fig. 7 differ, so do the shear rate profiles.

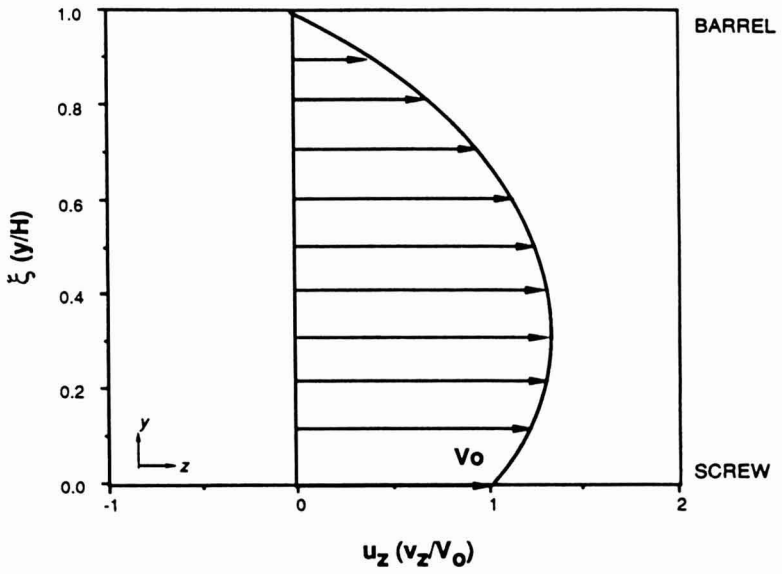

FIG. 7. VELOCITY PROFILE WHEN THE SCREW ROTATES AND THE BARREL REMAINS STATIONARY ($Q_P/Q_D = +1$)

If the screw rotates

$$v_z = V_o [\xi - 3\xi(1-\xi)(-1)] \tag{40}$$

then,

$$\frac{dv_z}{d\xi} = V_o [1+3-6\xi]. \tag{41}$$

and the shear rate obtained using Eq. (29) is,

$$\dot{\gamma} = \frac{V_o}{H} [4 - 6\xi] \tag{42}$$

At the screw surface ($\xi = 0$), $\dot{\gamma} = 4V_o/H$, while at the barrel surface ($\xi = 1$), $\dot{\gamma} = -2V_o/H$. The shear rates are, therefore, reverse from the case of the rotating barrel. In both cases though, the Newtonian fluid on the moving surface experiences twice the shear of the stationary surface.

Pressure Profile in the HSR

In the above analysis it was determined that since the only nonzero pressure gradient was dP/dz (dP/dx and dP/dy are zero) all the flow within the HSR was in the z-direction. As shown in Fig. 8a the z-direction is along the circumferential direction of the screw. Hence, the pressure sensed by a transducer on the stationary barrel increases linearly over a complete rotation. When the flight goes past the transducer, the pressure drops, and the cycle repeats itself resulting in a sawtoothed trace (Fig. 8b). Since there are isobars in the x-direction (direction of screw axis) the pressure at any point between two flights (A′ to B) is the same ($P_{A'} = P_B$). However, there is a pressure difference across the flights (A to A′) such that if

$$\Delta P = P_{A'} - P_A \tag{43}$$

then,

$$= P_B - P_A.$$

Thus, the pressure difference measured with two transducers at A and B is the same as the difference in pressure between A to A′ within the channel. Therefore, the traces from the two transducers at integral turns apart follow each other and

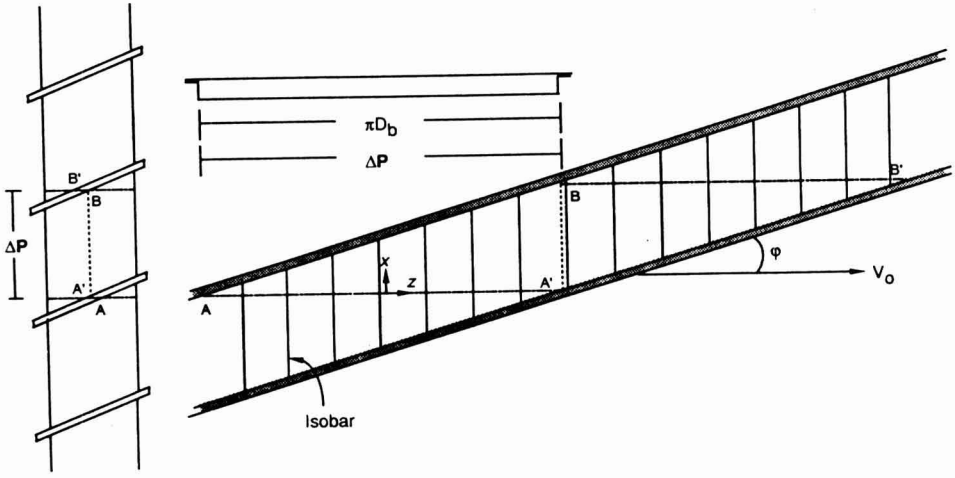

FIG. 8a. THE PRESSURE INCREASES LINEARLY IN THE CROSS-CHANNEL, A TO A′
The isobars in the x-direction make it possible to measure the same differential pressure along the axis of the screw between A′ and B′ since $\Delta P = P_A - P_B = P_B - P_A$.

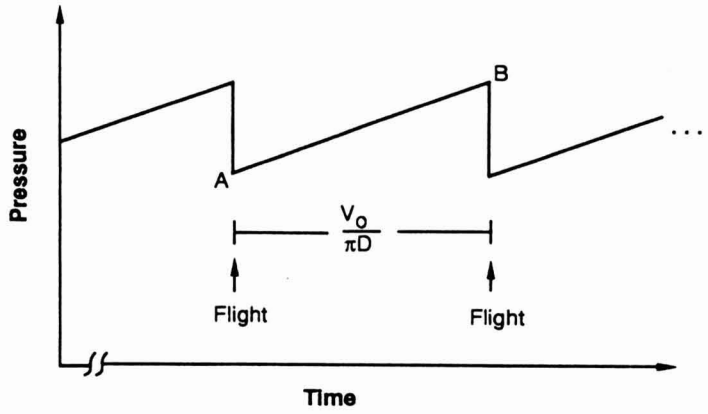

FIG. 8b. SAWTOOTH TRACE FROM A PRESSURE TRANSDUCER ON A STATIONARY BARREL SURFACE

the constant pressure offset between them is the same as the pressure range of the sawtoothed trace. If the transducers are two integral turns apart the offset would be twice as much.

The potential use of estimating viscosities in a single screw extruder was first suggested by Mohr and Mallouk (1959) but they considered it difficult to implement because the pressure gauges were believed to be dynamically too slow to measure the magnitude of the sawtooth trace. McKelvey and Wheeler (1963) later obtained experimental measurements of the dynamic pressure. The work reported here has shown the usefulness of the HSR as a transducer.

Differential Pressure Viscosity Calculation

The viscosity is calculated from Eq. (34) where

$$\frac{VoH}{2} = -\frac{H^3}{12\mu}\frac{dP}{dz} \tag{44}$$

is rearranged to,

$$\frac{\Delta P}{\Delta z} = -\frac{6\mu V_o}{H^2} \tag{45}$$

ΔP is the pressure differential within the channel (A to A′) and Δz corresponds to the channel width, πD. Note that ΔP is negative since the pressure downstream

is lower than the back pressure. Also, $V_o = \pi DN$ where N is the rotational rate. Thus, Eq. (45) becomes

$$\mu = -\frac{\Delta P}{N}\frac{H^2}{6\pi^2 D^2} \tag{46}$$

This equation is also valid for ΔP across one integral turn for reasons previously discussed. If ΔP is measured across more than one integral turn, the appropriate ΔP is obtained by dividing by the number of integral turns.

Slope Viscosity Calculation

Since the pressure trace from a single transducer increases linearly, it is possible to relate the linear part of the cycle to viscosity (McKelvey and Wheeler 1963). The distance, Δz, that the transducer moves relative to the screw in one cycle is the same as

$$\Delta z = V_o \Delta t \tag{47}$$

where Δt is the time it takes the screw for a complete rotation.
Hence, Eq. (45) can be rewritten as

$$\frac{\Delta P}{\Delta t} = -\frac{6\mu V_o^2}{H^2} \tag{48}$$

where $\Delta P/\Delta t$ is the slope of the regression of the pressure-time curve.

NEWTONIAN TWO-DIMENSIONAL RECTILINEAR FLOW ANALYSIS

The same simplifying assumptions as the previous one-dimensional analysis are used. The difference is in the positioning of the coordinate axes where the *z*-axis is in the down channel direction and the *x*-axis is perpendicular to the channel walls or the flights (Fig. 9). The fluid is considered with two velocity components — a cross channel component, v_x, and a down channel component, v_z. Hence, with this approach the entire unwrapped channel is considered in the flow analysis. The flow is assumed fully developed in the *z*- and the *x*-directions so $v_z = v_z(y)$ and $v_x = v_x(y)$. The down channel velocity v_z would also be a function of *x* if the effect of the flights are not neglected since the velocity at the walls is zero.

However, since a shallow channel is assumed ($H/W << 1$) the flight effects are neglected and an infinite channel is assumed. This analysis is the basis of classical extrusion theory (Carley *et al.* 1953; Weeks and Allen 1962; Squires 1964; Tadmor and Klein 1970).

Based on the above assumptions and definitions the components of the equation of motion reduce to

$$0 = -\frac{\partial P}{\partial z} - \frac{\partial \tau_{yz}}{\partial y} \qquad \text{(z-component)} \qquad (49)$$

$$0 = -\frac{dP}{dx} - \frac{\partial \tau_{yz}}{\partial x} \qquad \text{(x-component)} \qquad (50)$$

Substituting the Newtonian constitutive equations

$$\tau_{yz} = -\mu \frac{dv_z}{dy} \qquad (51)$$

$$\tau_{yx} = -\mu \frac{dv_x}{dy} \qquad (52)$$

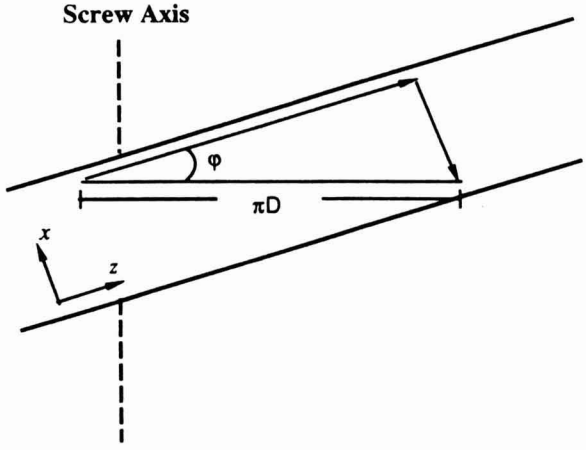

FIG. 9. HELICAL CHANNEL CONSIDERED IN THE TWO-DIMENSIONAL ANALYSIS

into the equations of motion results in

$$\frac{\partial P}{\partial z} = \frac{\partial^2 v_z}{\partial^2 y} \tag{53}$$

$$\frac{\partial P}{\partial x} = \frac{\partial^2 v_x}{\partial^2 y} \tag{54}$$

Since the left side of the equations (Eq. 53 and 54) depend on z only and the right side depends on y only, the equation can be integrated as an ordinary differential equation as before to obtain the velocity profiles. Then integrating the velocity profiles across the gap yields flow rates from which pressure differential-viscosity relationships can be obtained.

After simplifying and rearranging the same relationship as in the one-dimensional analysis is obtained (Eq. 46)

$$\mu = -\frac{\Delta P}{N}\frac{H^2}{6\pi^2 D^2} \tag{55}$$

If the wall effects were taken into account the z-component of the equation of motion would then be a partial differential equation

$$\frac{\partial P}{\partial z} = \mu \left[\frac{\partial^2 v_z}{\partial x^2} + \frac{\partial^2 v_z}{\partial y^2} \right] \tag{56}$$

The complete solution of the velocity profile in this rectangular channel was solved by Rowell and Finlayson (1922, 1928) and a detailed solution is also found in Booy (1963), Squires (1964) and Tadmor and Klein (1970). The solution consists of infinite series resulting in

$$Q = \left(\frac{\pi^2 D^2 NH}{2} \sin\varphi\cos\varphi\right) F_D - \left(\frac{\pi}{12\mu} \sin^2\varphi \; H^2 D \; \frac{\Delta P}{\Delta z}\right) F_P \tag{57}$$

The variation between the pressure (F_p) and drag(F_D) correction factors relative to the aspect ratio (H/W) for a square pitch screw have been determined by Tadmor and Gogos (1979). The drag factor was verified experimentally by Squires

(1964) but no verification of the pressure correction factor has been reported. If a shallow channel is assumed (H/W $<$ 0.1) the correction factors are very close to unity, so the previous assumption of v_z as a function of y only [vs. $v_z = v_z(x,y)$] was a reasonable assumption.

From the results of this two-dimensional analysis it can be shown that the axial component, v_l, as described by the vectorial summation of v_z and v_x.

$$v_l = -v_x \cos\varphi + v_z \sin\varphi \tag{58}$$

are in fact zero. Therefore, when there is no net flow through the channel there is no axial flow.

NEWTONIAN CYLINDRICAL DEEP CHANNEL FLOW ANALYSIS

A cylindrical coordinate system using z as in the axial direction, r in the radial direction, and θ in the circumferential direction, would seem to be a more natural choice for flow analysis of the HSR due to its geometry. This analysis was carried out and compared with the parallel plate shallow channel model (Tamura 1989). It was based mostly on Booy's development (Booy 1963) and a cylindrical analysis approximation is found in Tadmor and Klein (1970).

This analysis results in

$$\mu = \frac{\Delta P}{\Delta z}\frac{1}{N}\frac{R_o \tan\varphi_o}{8\pi}\frac{F(\alpha)}{K(\alpha)} \tag{59}$$

where $F(\alpha)$ and $K(\alpha)$ are functions of the ratio

$$\alpha = \frac{R_1}{R_o} \tag{60}$$

where R_1 is the barrel radius and R_0 is the radius of the root of the screw. This equation differs from that obtained in the rectilinear analysis by 6% (Tadmor and Klein 1970).

A comparison with the rectilinear flow rate (Eq. 57) is possible by rearranging the cylindrical flow rate into the following form

$$Q = F_{DC}\left(\frac{\pi}{2}(\sin\varphi_o \cos\varphi_o)\, H^2 D \frac{\Delta P}{\Delta z}\right) - F_{PC}\left(\frac{\pi}{12\mu}\sin^2\varphi_o\, H^3 D \frac{\Delta P}{\Delta z}\right) \tag{61}$$

where F_{DC} and F_{PC} are curvature factors. The curvature factors are significant at large helix angles and large aspect ratios. For the square pitch (17.6°) and shallow channel (H/D = 0.103) of the HSR the factors were $F_{DC} = 1.007$ and $F_{PC} = 1.043$; hence, the curvature effects can be considered relatively small.

NONNEWTONIAN ONE-DIMENSIONAL POWER-LAW FLOW ANALYSIS

The distinguishing characteristic of non-Newtonian fluids from Newtonian fluids is the dependence of viscosity on shear rate. In the Newtonian one-dimensional analysis the velocity profile for the HSR was determined to be nonlinear with both positive and negative shear rates. Since the fluid is sheared differently at the barrel surface from the screw root surface, it is necessary to determine the shear rate at the barrel surface where the pressure transducers are located to determine the apparent viscosities and/or the non-Newtonian fluid model parameters.

Different analyses can be found in Rotem and Shinnar (1961), Kroesser and Middleman (1965), Middleman (1965), Flumerflet *et al.* (1969), Zamodits and Pearson (1969), and Booy (1981). The non-Newtonian analysis outline here is based on the analysis by Tadmor and Gogos (1979) using the power law model but for the case of a rotating screw instead of a rotating barrel.

$$\tau_{yz} = -m \left| \frac{dv_z}{dy} \right|^{n-1} \left| \frac{dv_z}{dy} \right| \tag{62}$$

The Newtonian case is obtained when the power law index, n, equals 1 and the coefficient, m, is the Newtonian viscosity, μ.

The simplifying assumptions made in this analysis are the same as those made in the Newtonian analysis. Hence, the same equation of motion is used.

$$0 = -\frac{\partial P}{\partial z} - \frac{\partial \tau_{yz}}{\partial y} \tag{63}$$

Instead of substituting the Newtonian constitutive equation for τ, the power law model (Eq. 62) is substituted into the equation of motion to yield

$$\frac{\partial P}{\partial z} = m \frac{d}{dy} \left[\left| \frac{dv_z}{dy} \right|^{n-1} \frac{dv_z}{dy} \right] \tag{64}$$

The pressure gradient on the left side of the equation, $\partial P/\partial z$, is not a function of y, whereas the right side is only a function of y (Fig. 4b). The pressure gradient must, therefore, be constant, and the equation can be solved as an ordinary differential equation. Furthermore, by substituting the dimensionless variables

$$u_z = \frac{v_z}{V_o} \tag{65}$$

$$\xi = \frac{y}{H} \tag{66}$$

to Eq. (64) yields

$$\frac{dP}{dz} = \frac{m}{H}\left(\frac{V_o}{H}\right)^n \frac{d}{d\xi}\left[\left|\frac{du_z}{d\xi}\right|^{n-1}\frac{du_z}{d\xi}\right] \tag{67}$$

It is convenient to rearrange the above as

$$\frac{d}{d\xi}\left[\left|\frac{du_z}{d\xi}\right|^{n-1}\frac{du_z}{d\xi}\right] = \frac{H^{n+1}}{mV_o{}^n}\frac{dP}{dz} \tag{68}$$

Then, by defining the dimensionless parameter G as,

$$G = \frac{1}{6}\left[\frac{H^{n+1}}{mV_o}\frac{dP}{dz}\right] \tag{69}$$

Eq. (68) can be rewritten as

$$\frac{d}{d\xi}\left[\left|\frac{du_z}{d\xi}\right|^{n-1}\frac{du_z}{d\xi}\right] = 6G \tag{70}$$

Note that for the Newtonian case, G is equivalent to the dimensionless flow rate Q_P/Q_D (Eq. 25). That is, if n= 1 and m = μ.

$$G = \frac{1}{6}\left[\frac{H^{n+1}}{mV_o}\frac{dP}{dz}\right] = \frac{H^2}{6\mu V_o}\left[-\frac{dP}{dz}\right] \tag{71}$$

The constant G (as is Q_P/Q_D) is constant for a fluid since the pressure gradient increases linearly with increasing barrel rotation. Upon integrating Eq. (70)

$$\left|\frac{du_z}{d\xi}\right|^{n-1}\frac{du_z}{d\xi} = 6G\xi + K_1 \tag{72}$$

is obtained. We redefine the integration constant as

$$K_1 = -6G\lambda \tag{73}$$

where λ is the location of zero shear or the location of the extremum in the velocity profile. This is constant for a given fluid and is equal to ⅓ for Newtonian fluids. Substitution of K_1 into Eq. (72) yields

$$\left|\frac{du_z}{d\xi}\right|^{n-1}\frac{du_z}{d\xi} = 6G(\xi - \lambda) \tag{74}$$

From the above equation, four velocity profiles are possible as shown in Fig. 10. The first two cases, (I) and (II), are the only possible cases for the HSR where the extremums in velocity occur within the plate boundaries ($0 < \xi < 1$). Case (I) has a positive pressure gradient (increasing pressure in the direction of drag) and case (II) has a negative pressure gradient. Case (I) would occur when the screw is stationary while the barrel moved, while case (II) would be the opposite — the screw rotating with a stationary barrel.

Both profiles have positive and negative shear rates, so the absolute value in Eq. (74) cannot be eliminated easily. It is, therefore, necessary to subdivide the analysis of the profiles by considering the regions where $\xi > \lambda$ and $\xi < \lambda$ separately.

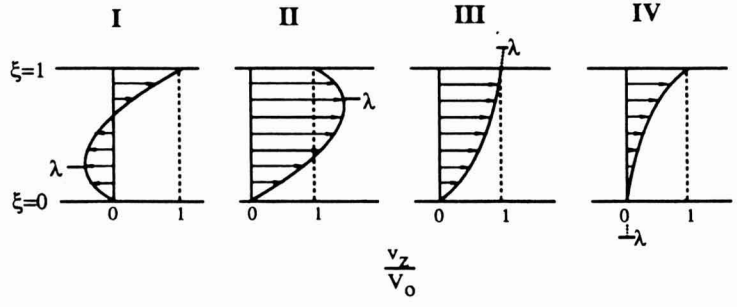

FIG. 10. VELOCITY PROFILES POSSIBLE BETWEEN PARALLEL PLATES WITH POWER LAW FLUIDS

First, the sign of the pressure gradient is tracked by letting

$$signG = \frac{G}{|G|} \tag{75}$$

The $signG$ is indicative of the direction of the pressure gradient (Eq. 71).

In case (I), both the shear rate and pressure gradient are positive in the region where $\xi \geqslant \lambda$ (Fig. 10). In case (II), the shear rate and the pressure gradient are negative. The absolute value can then be eliminated to obtain

$$\left(\frac{du_z}{d\xi}\right)^n = 6\, signG\, |G|\, (\xi-\lambda) \tag{76}$$

or

$$\frac{du_z}{d\xi} = |6G|^s (\lambda-\xi)^s signG \tag{77}$$

where

$$s = \frac{1}{n} \tag{78}$$

In the lower region where $\xi \geqslant \lambda$, case (I) consists of a negative shear rate and a positive pressure gradient. In case (II) the shear rate is positive while the pressure gradient is negative. Since λ is greater than ξ, Eq. (74) can be rewritten as

$$\frac{du_z}{d\xi} = -|6G|^s (\xi-\lambda)^s signG \tag{79}$$

The value of λ is evaluated by integrating the above equation with the following boundary conditions

$\xi \geq \lambda$: $\quad u_z = 1$ at $\xi = 1$

resulting in $\quad \xi \leq \lambda$: $\quad u_z = 0$ at $\xi = 0$

$$\xi \geq \lambda: \qquad u_z = 1 - \frac{|6G|^s}{s+1}\left[(1-\lambda)^{s+1} - (\xi-\lambda)^{s+1}\right] signG \tag{80}$$

$$\xi \leq \lambda: \qquad u_z = \frac{|6G|^s}{s+1}\left[(\lambda-\xi)^{s+1} - (\lambda)^{s+1}\right] signG \tag{81}$$

Since the velocity is continuous throughout the gap (ξ-direction) the velocity profiles [Eq. (80) and (81)] are equal at the velocity maxima. By setting both equations equal to each other and letting $\xi = \lambda$

$$1 - \frac{|6G|^s}{s+1}\left[(1-\lambda)^{s+1}\right] signG = \frac{|6G|^s}{s+1}\left[-(\lambda)^{s+1}\right] signG \tag{82}$$

or

$$0 = \lambda^{s+1} - (1-\lambda)^{s+1} + \frac{s+1}{|6G|^s signG} \tag{83}$$

The above equation, rewritten as

$$(1-\lambda)^{s+1} = \lambda^{s+1} + \frac{s+1}{|6G|^s signG} \tag{84}$$

is used to simplify Eq. (80) to obtain

$$u_z = 1 - \frac{|6G|^s}{s+1}\left[\left(\lambda^{s+1} + \frac{s+1}{|6G|^s signG}\right) - (\xi-\lambda)^{s+1}\right] signG \tag{85}$$

Furthermore, by transferring the negative sign inside the parenthesis,

$$u_z = 1 + \frac{|6G|^s}{s+1}\left[-\lambda^{s+1} - \frac{s+1}{|6G|^s signG}\right) + (\xi-\lambda)^{s+1}\right] signG \tag{86}$$

and then moving the "1" term inside the parenthesis,

$$u_z = \frac{|6G|^s}{s+1}\left[\frac{s+1}{|6G|^s signG} - \lambda^{s+1} - \frac{s+1}{|6G|^s signG}\right) + (\xi-\lambda)^{s+1}] \; signG \tag{87}$$

the equation is simplified to

$$u_z = \frac{|6G|^s}{s+1} signG \; [(\xi-\lambda)^{s+1} - \lambda^{s+1}] \tag{88}$$

The above equation can be combined with Eq. (81) using absolute value signs to obtain

$$u_z = \frac{|6G|^s}{s+1} signG \; [|\xi-\lambda|^{s+1} - \lambda^{s+1}] \tag{89}$$

The flow rate per unit depth can now be determined with

$$\frac{Q}{V_o H} = \int_0^1 u_z \, d\xi \tag{90}$$

which results in

$$Q = V_o H \frac{|6G|^s}{s+1} signG \left[\frac{(1-\lambda)^{s+2}}{s+2} - \lambda^{s+1} + \frac{\lambda^{s+2}}{s+2}\right] \tag{91}$$

As in the Newtonian case analysis, for a viewer fixed on the barrel the net flow is $Q = V_o H$. Hence,

$$V_o H = V_o H \frac{|6G|^s}{s+1} signG \left[\frac{(1-\lambda)^{s+2}}{s+2} - \lambda^{s+1} + \frac{\lambda^{s+2}}{s+2}\right] \tag{92}$$

Simplifying and rearranging, yields the polynomial

$$0 = \frac{(1-\lambda)^{s+2}}{s+2} + \frac{\lambda^{s+2}}{s+2} - (1-\lambda)^{s+1} \tag{93}$$

or

$$0 = (1-\lambda)^{s+2} + \lambda^{s+2} - (s+2)(1-\lambda)^{s+1} \tag{94}$$

However, if the barrel were rotated the net flow rate is zero (Q = 0) and Eq. (92) would yield a different polynomial

$$0 = (1-\lambda')^{s+2} + \lambda'^{s+2} - (s+2)(\lambda')^{s+1} \tag{95}$$

where λ and λ' are related by

$$\lambda = 1-\lambda' \tag{96}$$

The relationship between λ, n, and G are shown in Fig. 11.

Power Law Parameter Calculation

As suggested by Kraynik (1984a) the parameter n can be determined from the logarithmic fit of Eq. (69), rearranged here as

$$\frac{V_o^n}{H^n} = \frac{H\ dP/dz}{6mG} \tag{97}$$

such that

$$n \log(\frac{V_o}{H}) = \log(\frac{HdP}{dz}) - \log(6mG) \tag{98}$$

$$n = \frac{d\log(HdP/dz)}{d\log(V_o,H)} \tag{99}$$

Hence, with this equation, n can be determined from measured pressure gradients at various screw speeds. After determining n, the root of Eq. (94) can be found to obtain λ. The dimensionless parameter G is then obtained from Eq. (83)

$$6G = \left(\frac{s+1}{[(1-\lambda)^{s+1} - \lambda^{s+1}]signG}\right)^n \tag{100}$$

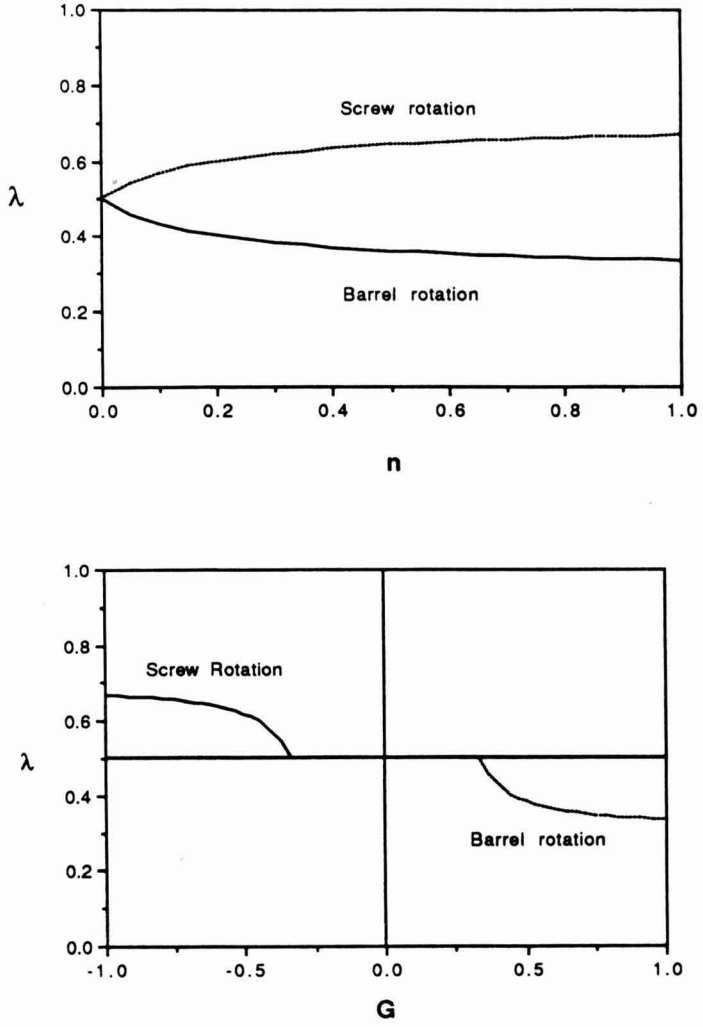

FIG. 11. RELATIONSHIP BETWEEN POWER LAW PARAMETER, n, AND DIMENSIONLESS VARIABLES λ AND G

The parameter m is determined also with Eq. (69)

$$m = \frac{H^{n+1}}{6V_o{}^n G} \frac{dP}{dz} \tag{101}$$

The shear rate is then determined using Eq. (89)

$$\dot{\gamma} = \frac{dv_z}{dy} = \frac{V_0}{H}\frac{du_z}{d\xi} = \frac{V_0}{H}\left(-|6G|^s(\lambda-\xi)^s signG\right) \tag{102}$$

CONCLUSION

Newtonian and non-Newtonian fluids have been considered separately. For Newtonian fluids the velocity profile and flow rate were determined from the equation of motion and a mass balance. A simple relationship between the desired viscosity and the measured pressure differential was obtained. For the non-Newtonian case, the same basic approach was taken but, in addition, it was necessary to also determine the shear rate profile in order to obtain the parameters of the power-law model.

It is important to note that in general extrusion theory, the barrel has always been assumed to be the rotating element for ease in analysis, since it makes no difference whether the barrel or the screw rotates. That is, if the barrel rotates, it is the same as if the screw rotates in the opposite direction while the observer also rotates with the screw. However, if the screw rotates and the observer is stationary with the barrel, the velocity profile will differ and this was shown in the analysis. This distinction is necessary in the shear rate profile analysis because the shear rate is nonlinear across the gap. In previous analyses, an average shear rate across the gap was adequate for extruder applications, but the shear rate at the wall of the outside barrel is of specific interest for the HSR.

For a square pitched HSR the theoretical analysis suggests that a one-dimensional rectilinear analysis is adequate to determine rheological parameters. Complex flow effects near the flights can be minimized as long as a narrow gap between the screw and barrel is maintained.

ACKNOWLEDGMENTS

The authors thank the California League of Food Processors for taking interest in this project and providing funding.

SYMBOLS

D	Barrel or screw diameter
ΔP	Pressure differential
F_{DC}, F_{PC}	Pressure and drag curvature correction factors
F_D, F_P	Pressure and drag correction factors

Symbols (*cont.*)

g	Gravitational acceleration tensor
G	Dimensionless parameter in Power Law analysis
H	Screw channel depth
m	Consistency index, power law model
N	Rotation rate
n	Flow behavior index, power law model
P	Pressure tensor
Q_D	Flow rate due to drag
Q_P	Flow rate due to pressure
s	1/n
t	Time
u_z	Dimensionless velocity
v	Velocity vector
V_o	Velocity of screw or barrel
W	channel width

Greek Letters

α	Ratio of barrel to inner cylinder radius
ξ	Dimensionless channel depth
γ	Shear
$\dot{\gamma}$	Shear rate (s^{-1})
λ	Position of velocity profile maxima
λ'	$= 1 - \lambda$
μ	Viscosity (dynes-s/cm^2)
ρ	Fluid density
τ	Shear stress (dynes/cm^2)
τ_o	Shear stress at screw surface
τ	Stress tensor

REFERENCES

BIRD, R.B., STEWART, W.E. and LIGHTFOOT, E.N. 1960. *Transport Phenomena*, John Wiley & Sons, New York.

BOOY, M.L. 1963. Influence of channel curvature on flow, pressure distribution, and power requirements of screw pumps and melt extruders. SPE Trans. *3*, 176–185.

BOOY, M.L. 1981. The influence of non-Newtonian flow on effective viscosity and channel efficiency in screw pumps. Polym. Eng. Sci. *21*(2), 93–99.

CARLEY, J.F., MALLOUK, R.S. and MCKELVEY, J.M. 1953. Simplified flow theory for screw extruders. Ind. Eng. Chem. *45*(5), 974–978.

FLUMERFELT, R.W., PIERICK, M.W., COOPER, S.L. and BIRD, R.B. 1969. Generalized plane couette Flow of a non-Newtonian. Fluid Ind. Eng. Chem. Fundam. *8*(2), 354–357.

HOLDSWORTH, S.D. 1971. Applicability of rheological models to the interpretation of flow and processing behaviour of fluid food products. J. Texture Studies *2*, 393–418.

KRAYNIK, A.M., AUBERT, J.H. and CHAPMAN, R.N. 1984a. The Helical Screw Rheometer. Proc. IX Intl. Congress on Rheology, Mexico 77–84.

KRAYNIK, A.M. AUBERT, J.H., CHAPMAN, R.N. and GYURE, D.C. 1984b. The Helical Screw Rheometer: A new concept in rotational rheometry. ANTEC, 405–408.

KROESSER, F.W. and MIDDLEMAN, S. 1965. The calculation of screw characteristics for the extrusion of non-Newtonian melts. Poly. Eng. Sci. *5*, 230–234.

MCKELVEY, J.M. 1962. *Polymer Processing*, John Wiley & Sons, New York.

MCKELVEY, J.M. and WHEELER, JR., N.C. 1963. Analysis of pressure transducer data from screw extruders. SPE Trans. *3*, 138–144.

MIDDLEMAN, S. 1965. Flow of power law fluids in rectangular ducts. Trans. Soc. Rheol. *9*(1), 83–93.

MOHR, W.D. and MALLOUK, R.S. 1959. Flow, Power Requirement, and Pressure Distribution of Fluid in a Screw Extruder. Ind. Eng. Chem. *51*(6), 765–770.

PEARSON, J.R.A. 1985. *Mechanics of Polymer Processing*, Elsevier Applied Science Publ. Ltd., London.

RAO, M.A. 1977a. Rheology of liquid foods: A review. J. Texture Studies *8*, 135–168.

RAO, M.A. 1977b. Measurement of flow properties of fluid foods: Developments, limitations, and interpretation of phenomena. J. Texture Studies *8*, 257–282.

RAUWENDAAL, C. 1986. *Polymer Extrusion*, Macmillan Publishing Co., New York.

ROTEM, Z. and SHINNAR, R. 1961. Non-Newtonian flow between parallel boundaries in linear movement. Chem. Eng. Sci. *15*, 130–143.

ROWELL, H.S. and FINLAYSON, D. 1922. Screw Viscosity Pumps. Eng. *114*, 606–607.

ROWELL, H.S. and FINLAYSON, D. 1928. Screw viscosity pumps. Engineering *126*, 249–250.

SQUIRES, P.H. 1964. Screw extrusion: Flow patterns and recent theoretical developments. SPE Trans. *4*, 7–16.

TADMOR, Z. and GOGOS, C.G. 1979. *Principles of Polymer Processing*, John Wiley & Sons, New York.

TADMOR, Z. and KLEIN, I. 1970. *Engineering Principles of Plasticating Extrusion*, Van Nostrand Reinhold Co., New York.

TAMURA, M.T. 1989. Evaluation of the Helical Screw Rheometer for Fluid Food Suspensions. Ph.d. Thesis, University of California, Davis.

TILY, P.J. 1983. Viscosity measurement (Part 2). Meas. Control *16*, 137–139.

VAN WAZER, J.R., LYONS, J.W., KIM, K.Y. and COLWELL, R.E. 1963. *Viscosity and Flow Measurement A Laboratory Handbook*, Interscience Publishers, New York.

WEEKS, D.J. and ALLEN, W.J. 1962. Screw extrusion of plastics. J. Mech. Eng. Sci. *4*(4), 380–400.

WHORLOW, 1980. *Rheological Techniques*, John Wiley & Sons, New York.

ZAMODITS, H.J. and PEARSON, J.R.A. 1969. Flow of polymer melts in extruders. Part I. The effect of transverse flow and of a superposed steady temperature profile. Trans. Soc. Rheol. *13*(3), 357–385.

A GRID GENERATION TECHNIQUE FOR NUMERICAL MODELLING HEAT AND MOISTURE MOVEMENT IN PEAKED BULKS OF GRAIN

A.K. SINGH

Department of Civil and Agricultural Engineering
University of Melbourne, Parkville, Victoria, Australia 3052

and

G.R. THORPE

Department of Civil and Building Engineering
Victoria University of Technology, Footscray, Victoria, Australia 3011

Accepted for Publication December 21, 1992

ABSTRACT

This paper describes a numerical solution procedure to study heat and moisture transfer processes by two-dimensional natural convection phenomena in grain stores with arbitrary geometries. This enables grain storage technologists to investigate the design and performance of grain stores in which the grain surface is peaked, as in bunker storage, for example. Momentum transfer is described by an elliptic partial differential equation, which governs the behavior of the stream function. Using an algebraic grid generation technique, the governing equations are transformed into a body-fitted rectangular coordinate system that allows coincidence of all boundary lines with a coordinate line. Numerical solutions of the resulting equations are obtained using an alternating direction implicit method. Results from numerical experiments on a peaked bulk of stored grain retained between two vertical walls are obtained that show the magnitude and directions of convection currents and contours of temperature, moisture, dry matter loss and chemical pesticide concentrations.

Journal of Food Process Engineering **16** (1993) 127–145.

INTRODUCTION

The size of harvests of food grains varies considerably from season to season. The construction of permanent grain stores to handle the entire crop in years of bountiful harvest may not be an efficient use of capital. An alternative to permanent stores is to store grains in bunkers in which grains are heaped on an impermeable floor and covered with tarpaulins designed to exclude moisture and rodents. The grain may be kept in place by small retaining walls. Yates and Sticka (1984) outline the development of bunker stores that are now routinely constructed with capacities of 50,000 tonnes of wheat.

One potential problem associated with bunker stores is moisture migration. When cereal grains are harvested in Australia they have temperatures of typically 30C (Griffiths 1964) and an upper limit on grain moisture content of 12% (wet basis) is set by the grain handling authorities. While grains may be safely stored for prolonged periods of time at this moisture content, there is a possibility that moisture will be redistributed within the grain bulk as a result of natural convection currents, as illustrated by the work of Thorpe and Nguyen (1987), for example. Because of the large thermal mass of a bulk of grain, the central region cools down slowly. However, the surfaces cool as winter approaches and the temperature gradients normal to the gravitational field set up convection currents. Air with a relatively high absolute humidity rises into the cooler regions whence its relative humidity increases, thus causing the grains to adsorb moisture. Molds and insects can flourish in such high moisture content grain and the grains may be so damaged that they are of no commercial value.

A first step in the engineering design of bunker grain stores so that problems associated with moisture migration may be ameliorated is to formulate the equations that govern moisture and heat transfer within grain bulks. Thorpe *et al.* (1992) have derived the partial differential equations that govern heat, mass and momentum transfer in bulk stored grains. They must be solved with the appropriate initial conditions, such as grain moisture content and temperature, and boundary conditions such as the surface temperature of the grain and the impermeability of the tarpaulin to moisture. An exact solution of the nonlinear equations is quite intractable and numerical methods must be used. Thorpe and Nguyen (1987) presented a method of solving the governing equations in grain stores with simple geometries. In these studies it was possible to demonstrate the effects of convection currents on the redistribution of moisture in the bulk and the effects of the rate of cooling on the decay of chemical pesticides and insect mortality. Nguyen (1987) presented a model of heat and moisture transfer in bunker stores in which the numerical grid points were coincident with the upper surface of the grain. The boundary condition expressing the conservation of mass was not explicitly stated by the author and to this extent the model may be considered to be in-

complete. Freer *et al.* (1990) used Nguyen's (1987) model to investigate moisture migration in bunkers containing rice.

The aim of this research is to present a numerical scheme for dealing with bulks of grain that are peaked, or indeed have any geometrical cross section. The numerical procedure enables zero-flux boundary conditions that govern the behavior of moisture vappor at the impermeable boundaries to be treated in a straightforward manner. Furthermore, the procedure outlined in this paper is readily extended to three-dimensional geometries by replacing the stream function formulation with a vector potential after the manner of Mallinson and de Vahl Davis (1973). The idea behind the method is to transform a system with a complicated geometry into one that is simple, i.e., a square or a cube. In systems with such simple geometries it is possible to discretize the governing differential equations on orthogonal grids. In this way, complicated problems are reduced to those that have well-known and standard methods of solution. The method has been successfully employed by Saitoh (1978), Lee (1984), Shyy *et al.* (1985), Chen *et al.* (1990), and Chiu and Wu (1990) to solve flow problems corresponding to an arbitrary domain. Darcy's law is used to account for momentum transfer in the grain bulk, and momentum equations are expressed in terms of the stream function instead of velocity and pressure in order to simplify the numerical procedure. A finite-difference solution of the transformed equations in the computational domain is obtained by using an alternating direction implicit method (ADI) in terms of stream function, moisture content of the grain and temperature and the numerical results obtained are shown in the form of contours.

GOVERNING EQUATIONS

The governing equations for describing flow formation in a hygroscopic porous medium, such as a bulk of stored grains, consist of mass, momentum, moisture and thermal energy balances, which in sequence are as follows:

Mass continuity equation:

$$\nabla' \cdot \mathbf{V}' = 0, \tag{1}$$

Darcy's law:

$$\mathbf{V}' = -\frac{K}{\mu}\left(\nabla' p' + \rho_f \mathbf{g}\right), \tag{2}$$

Moisture balance equation:

$$\rho_s \frac{\partial W}{\partial t'} + \rho_f \mathbf{V}' \cdot \nabla' w = \rho_f D_{eff} \nabla'^2 w + \rho_s q_w \frac{\partial d_m}{\partial t'}, \tag{3}$$

Thermal energy balance equation:

$$\rho_s C_s \frac{\partial T'}{\partial t'} + \rho_f C_f V' \cdot \nabla' T' + \rho_f (C_w + \frac{\partial h_v}{\partial T'})(wV' - D_{eff} \nabla' w) \cdot \nabla' T' =$$

$$\kappa_{eff} \nabla'^2 T' + \rho_s h_s \frac{\partial W}{\partial t'} + \rho_s q_H \frac{\partial d_m}{\partial t'}, \tag{4}$$

where

$$C_s = C_m + C_w W. \tag{5}$$

Under the assumption of the Boussinesq approximation, the density of intergranular air is taken to be constant everywhere except in the buoyancy force term of the Darcy equation Eq. (2) satisfying the following linear state equation:

$$\rho_f = \rho_{of}[1 - \beta (T' - T'_o)]. \tag{6}$$

A detailed derivation of Eq. (3) and (4) is given by Thorpe *et al.* (1992).

The physical domain of the model is an arbitrary cavity in which grains are stored initially at temperature T'_g. The x′-axis is taken to be along floor of the grain store and y′-axis normal to it. The rigid side walls at x′ = 0, L and the top boundary are kept at constant temperature T'_o. The rigid floor is thermally insulated. For a two dimensional model, it is convenient to obtain the solution in terms of a stream function instead of primitive quantities. By defining the stream function as

$$u' = \frac{\partial \psi'}{\partial y'}, \qquad v' = -\frac{\partial \psi'}{\partial x'}, \tag{7, 8}$$

the mass continuity equation is automatically satisfied, and eliminating the pressure term from the momentum Eq. (2) by cross differentiation and using Eq. (6), we get

$$\frac{\partial^2 \psi'}{\partial x'^2} + \frac{\partial^2 \psi'}{\partial y'^2} = -\frac{K \rho_{of} \beta g}{\mu} \frac{\partial T'}{\partial x'}. \tag{9}$$

Before proceeding further, it is convenient for mathematical analysis to bring these equations into nondimensional form and hence we define nondimensional quantities as

$$t = t'/(\rho_f C_f H^2/\kappa_{eff}), \quad (x, y)=(x', y')/H, \quad (u, v) = (u', v')/(\kappa_{eff}/H\rho_f C_f),$$

$$T = (T' - T'_o)/\Delta T', \qquad \psi = \psi'/(\kappa_{eff}/\rho_f C_f). \tag{10}$$

The ratio of the width of the bunker to the height of the retaining walls, W/H, is designated by Arx. In view of Eq. (10), Eq. (9) and equations obtained from Eq. (3) and Eq. (4) corresponding to two-dimensional case are transformed into

$$\frac{\partial^2 \psi}{\partial x^2} + \frac{\partial^2 \psi}{\partial y^2} = - Ra \frac{\partial T}{\partial x}, \tag{11}$$

$$\frac{\partial W}{\partial t} + w_i \left(u \frac{\partial w}{\partial x} + v \frac{\partial w}{\partial y}\right) = w_i w_d \left(\frac{\partial^2 w}{\partial x^2} + \frac{\partial^2 w}{\partial y^2}\right) + q_w \frac{\partial d_m}{\partial t}, \tag{12}$$

$$\frac{\partial T}{\partial t} + t_i \left(u \frac{\partial T}{\partial x} + v \frac{\partial T}{\partial y}\right) + t_w \left[(wu - w_d \frac{\partial w}{\partial x}) \frac{\partial T}{\partial x} + (wv - w_d \frac{\partial w}{\partial y}) \frac{\partial T}{\partial y}\right] =$$

$$t_d \left(\frac{\partial^2 T}{\partial x^2} + \frac{\partial^2 T}{\partial y^2}\right) + \frac{1}{C_s \Delta T'} \left(h_s \frac{\partial W}{\partial t} + q_H \frac{\partial d_m}{\partial t}\right), \tag{13}$$

where

$$w_i = \rho_f / \rho_s, \qquad w_d = \rho_f C_f D_{eff} / \kappa_{eff},$$

$$t_i = t_d = \rho_f C_f / \rho_s C_s, \qquad t_w = \frac{w_i}{C_s} \left(C_w + \frac{\partial h_v}{\partial T'}\right). \tag{14}$$

The Darcy-Rayleigh number, Ra is defined in the usual way by

$$Ra = \beta K g \rho_f^2 C_f \Delta T' H / \mu \kappa_{eff}. \tag{15}$$

All of the boundaries are deemed to be impermeable to moisture vapor, in which case the air moisture content gradient normal to the boundaries is zero. The stream function is constant along the boundaries and is known to an arbitrary constant at the periphery of the grain store where it is set to zero. The dimensionless temperature of the sides and upper surfaces of the bunker are set to zero, and the floor is assumed to be adiabatic. The corresponding boundary conditions expressed in dimensionless quantities are:

$$\psi = \frac{\partial w}{\partial \mathbf{n}} = 0 \quad \text{on all boundaries;} \tag{16a}$$

$$T = 0 \quad \text{at} \quad f_1(x, y) = f_2(x, y) = f_4(x, y) = 0; \tag{16b}$$

$$\frac{\partial T}{\partial y} = 0 \quad \text{at} \quad f_3(x, y) = 0; \tag{16c}$$

where n is the normal vector and the functions f_1, f_2, f_3, and f_4 represent boundaries of the considered physical domain as shown in Fig. 1(a).

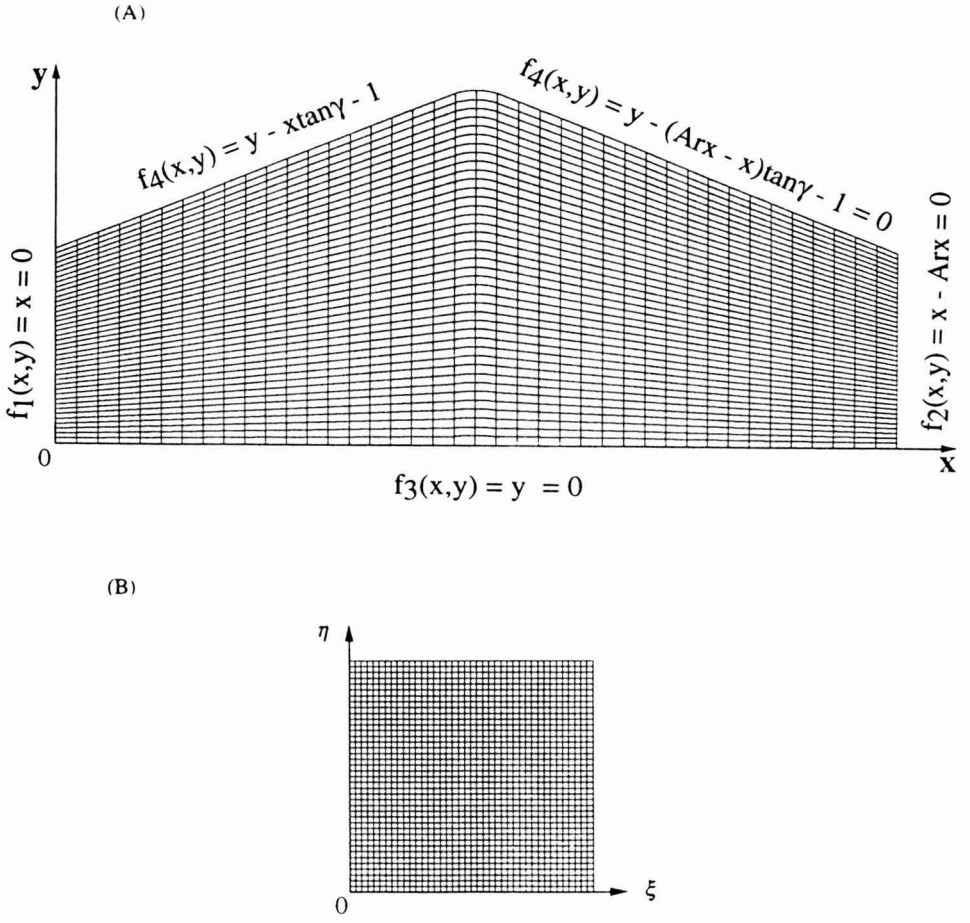

FIG. 1. GRID POINTS IN THE PHYSICAL DOMAIN (A) AND THE COMPUTATIONAL DOMAIN (B)

EQUATIONS IN THE COMPUTATIONAL DOMAIN

The first step in the grid generation technique is to define a transformation of the coordinate system which transforms the physical domain into a computational domain. In the case of a two-dimensional domain, as shown in Fig. 1(a, b), two dependent variables (ξ, η) can be used to transform the governing equations from the physical domain into the computational domain, in which (x, y) represent points in the physical domain while (ξ, η) represent points in the computational domain. According to Moretti and Abbett (1966), ξ and η are considered as follows:

$$\xi = \frac{x - f_1(x, y)}{f_2(x, y) - f_1(x, y)}, \tag{17}$$

$$\eta = \frac{y - f_3(x, y)}{f_4(x, y) - f_3(x, y)}. \tag{18}$$

Therefore

$$\xi = \xi(x, y), \quad \eta = \eta(x, y), \tag{19}$$

and conversely

$$x = x(\xi, \eta), \quad y = y(\xi, \eta). \tag{20}$$

In the Eq. (17) and (18), the functions f_1 to f_4 describing boundaries of the grain store can be taken as any analytical function or even in the form of numerical values prescribed at the boundaries. Using this set of transformations, explicit functional relationships between the physical and computational domains can be obtained. For evaluating x and y, Eq. (17) and (18) can be written as

$$x = f_2(\eta)\ \xi + f_1(\eta)\ (1 - \xi) \tag{21}$$

$$y = f_4(\xi)\ \eta + f_3(\xi)\ (1 - \eta) \tag{22}$$

As we have to perform all numerical computations in the computational domain, the original partial differential equations as well as boundary conditions are transformed from the physical domain (x, y) to the computational domain (ξ, η) by applying the following chain rule of partial differentiation:

$$\frac{\partial \phi}{\partial x} = \frac{\partial \phi}{\partial \xi}\frac{\partial \xi}{\partial x} + \frac{\partial \phi}{\partial \eta}\frac{\partial \eta}{\partial x}, \tag{23}$$

$$\frac{\partial \phi}{\partial y} = \frac{\partial \phi}{\partial \xi}\frac{\partial \xi}{\partial y} + \frac{\partial \phi}{\partial \eta}\frac{\partial \eta}{\partial y}, \tag{24}$$

where ϕ represents any function of x and y.

In terms of these new variables (ξ, η), the governing Eq. (11) to (13) obtained by applying the chain rule of differentiation given by Eq. (23) and (24) and followed by some algebraic manipulations, can be written as

$$\beta_1 \frac{\partial^2 \psi}{\partial \xi^2} + \beta_2 \frac{\partial^2 \psi}{\partial \eta^2} + \beta_3 \frac{\partial^2 \psi}{\partial \xi \partial \eta} + \beta_4 \frac{\partial \psi}{\partial \xi} + \beta_5 \frac{\partial \psi}{\partial \eta} = -\,\mathrm{Ra}\left(\alpha_1 \frac{\partial T}{\partial \xi} + \alpha_2 \frac{\partial T}{\partial \eta}\right), \tag{25}$$

$$\frac{\partial W}{\partial t} + w_i\,(\alpha_1 u + \alpha_3 v - \beta_4 w_d)\frac{\partial w}{\partial \xi} + w_i\,(\alpha_2 u + \alpha_4 v - \beta_5 w_d)\frac{\partial w}{\partial \eta} =$$

$$w_i w_d \left(\beta_1 \frac{\partial^2 w}{\partial \xi^2} + \beta_2 \frac{\partial^2 w}{\partial \eta^2} + \beta_3 \frac{\partial^2 w}{\partial \xi \partial \eta}\right) + q_w \frac{\partial d_m}{\partial t}, \tag{26}$$

$$\frac{\partial T}{\partial t} + \{\alpha_1(t_i u + t_{mx}) + \alpha_3(t_i v + t_{my}) - \beta_4 t_d\}\frac{\partial T}{\partial \xi}$$

$$+ \{\alpha_2(t_i u + t_{mx}) + \alpha_4(t_i v + t_{my}) - \beta_5 t_d\}\frac{\partial T}{\partial \eta} =$$

$$t_d \left(\beta_1 \frac{\partial^2 T}{\partial \xi^2} + \beta_2 \frac{\partial^2 T}{\partial \eta^2} + \beta_3 \frac{\partial^2 T}{\partial \xi \partial \eta}\right) + \frac{1}{C_s \Delta T'}\left(h_s \frac{\partial W}{\partial t} + q_H \frac{\partial d_m}{\partial t}\right). \tag{27}$$

The quantities α_1, α_2, . . . β_5, t_{mx} and t_{my} are defined as

$$\alpha_1 = \frac{\partial \xi}{\partial x}, \quad \alpha_2 = \frac{\partial \eta}{\partial x}, \quad \alpha_3 = \frac{\partial \xi}{\partial y}, \quad \alpha_4 = \frac{\partial \eta}{\partial y},$$

$$\beta_1 = \alpha_1^2 + \alpha_3^2, \quad \beta_2 = \alpha_2^2 + \alpha_4^2, \quad \beta_3 = 2(\alpha_1 \alpha_2 + \alpha_3 \alpha_4),$$

$$\beta_4 = 2\left(\frac{\partial^2 \xi}{\partial x^2} + \frac{\partial^2 \xi}{\partial y^2}\right), \quad \beta_5 = 2\left(\frac{\partial^2 \eta}{\partial x^2} + \frac{\partial^2 \eta}{\partial y^2}\right),$$

$$t_{mx} = t_w[u\, w - w_d(\alpha_1 \frac{\partial w}{\partial \xi} + \alpha_2 \frac{\partial w}{\partial \eta}),$$

$$t_{my} = t_w[v\, w - w_d(\alpha_3 \frac{\partial w}{\partial \xi} + \alpha_4 \frac{\partial w}{\partial \eta}). \tag{28}$$

The new terms appearing in these equations represent source terms in the computational domain that result from the transformation of the physical domain into the computational domain. The velocity components are computed from the expressions

$$u = \alpha_3 \frac{\partial \psi}{\partial \xi} + \alpha_4 \frac{\partial \psi}{\partial \eta}, \quad v = -(\alpha_1 \frac{\partial \psi}{\partial \xi} + \alpha_2 \frac{\partial \psi}{\partial \eta}). \tag{29}$$

It should be noted that nontransformed equations can be easily reestablished by setting $\alpha_1 = \alpha_4 = 1$, and $\alpha_2 = \alpha_3 = \beta_4 = \beta_5 = 0$. Thus, the transformation relation can be easily removed for problems where it is not needed.

The physical boundary conditions after transforming into the computational domain are as follows:

$$\psi = 0 \quad \text{on all boundaries;} \tag{30a}$$

$$T = 0 \quad \text{at} \quad \xi = 0, 1 \quad \text{and} \quad \eta = 1; \tag{30b}$$

$$\alpha_3 \frac{\partial T}{\partial \xi} + \alpha_4 \frac{\partial T}{\partial \eta} = 0 \quad \text{at} \quad \eta = 0; \tag{30c}$$

$$\alpha_1 \frac{\partial w}{\partial \xi} + \alpha_2 \frac{\partial w}{\partial \eta} = 0 \quad \text{at} \quad \xi = 0, 1; \tag{30d}$$

$$\alpha_3 \frac{\partial w}{\partial \xi} + \alpha_4 \frac{\partial w}{\partial \eta} = 0 \quad \text{at} \quad \eta = 0; \tag{30e}$$

$$(\alpha_1 n_x + \alpha_3 n_y) \frac{\partial w}{\partial \xi} + (\alpha_2 n_x + \alpha_4 n_y) \frac{\partial w}{\partial \eta} = 0 \quad \text{at} \quad \eta = 1; \tag{30f}$$

where n_x and n_y are the direction cosines of the outward normal of the boundary $f_4(x, y) = 0$. The set of differential Eq. (25) to (27) and boundary conditions (30) comprise the mathematical statement of the problem in the computational domain. Having transformed in this way the governing equations and the boundary conditions defined in the physical domain to those in the computational domain, we now describe in brief the method of solution of the transformed equations in the computational domain.

NUMERICAL SOLUTION

In the numerical procedure, the solution region as given in Fig. 1(a) is transformed into a rectangular domain as shown in Fig. 1(b) by specifying the functions f_1, f_2, f_3, and f_4 in Eq. (17) and (18). The governing equations are discretized by using a central difference for space derivatives and forward difference for the time derivative. The resulting finite difference equation corresponding to Eq. (27) is then solved by the alternating direction implicit method (ADI) described by Peaceman and Rachford (1955) and Douglas and Rachford (1956). Detailed accounts of the methods are given by de Vahl Davis (1976). In doing so, the mixed spatial derivative emerging due to transformation is treated by considering it as a source term.

The solution of Eq. (25), a general Poisson equation in the two-dimensional case, can be obtained by an iteration method. A drawback of this method is that a large number of iterations is required to achieve accurate results. This iteration process can be reduced in magnitude by formulating the problem as being pseudo-transient by adding a false time-dependent term $\partial\psi/\partial t$ as proposed by Mallinson and de Vahl Davis (1973). Thus, the procedure for obtaining the steady state solution of the stream function is to cast Eq. (25) is parabolic form, i.e.,

$$\frac{1}{\alpha_\psi}\frac{\partial \psi}{\partial t} = \beta_1 \frac{\partial^2 \psi}{\partial \xi^2} + \beta_2 \frac{\partial^2 \psi}{\partial \eta^2} + \beta_3 \frac{\partial^2 \psi}{\partial \xi \partial \eta} + \beta_4 \frac{\partial \psi}{\partial \xi} + \beta_5 \frac{\partial \psi}{\partial \eta}$$

$$+ \mathrm{Ra}\left(\alpha_1 \frac{\partial T}{\partial \xi} + \alpha_2 \frac{\partial T}{\partial \eta}\right), \tag{31}$$

with the introduction of a false transient term, in which α_ψ is false transient parameter with an arbitrary value determined by numerical experiments. As the stream function is obtained by a false transient method, the solution procedure corresponding to Eq. (31) is iterated to a steady-state solution unless the criterion

$$\frac{\sum\sum_{i\,j} |\psi_{i,j}^{k+1} - \psi_{i,j}^{k}|}{\sum\sum_{i\,j} |\psi_{i,j}^{k+1}|} < \psi_{err}, \tag{32}$$

is achieved in every time step, where ψ_{err} is maximum permissible error allowed in numerical calculations. The superscripts k and (k+1) indicate the value of the k^{th} and $(k+1)^{th}$ iterations, respectively, while indices i and j represent grid locations in the (ξ, η) plane.

As is evident from Eq. (26), to update the grain moisture content at each point in the bed with respect to a new temperature field it is necessary to obtain the moisture content of intergranular air at the new temperature. To achieve this requirement, the sorption isotherm equations and methodology proposed by Hunter (1987) have been used. Knowing the moisture content of the air, Eq. (26) is used to obtain the moisture content of grain.

Thompson (1972) reported that the dry matter loss, d_m in stored maize depends upon grain moisture content, temperature and time and the empirical relations he presented are used here to fulfill those requirements. However, for obtaining the rate of pesticide decay in a grain store, the relationship between pesticide concentration, temperature of grain, relative humidity of intergranular air and time given by Thorpe (1986) as

$$C_{pes} = C_i \exp[-1.3863 rt' \times 10^{B(T' - 30)/t^*}] \tag{33}$$

is used in which B and t* are pesticide-specific empirical constants having values 0.036 and 8.467×10^6, respectively, for the pesticide fenitrothion as reported by Desmarchelier and Bengston (1979) and C_i is the initial concentration of the pesticide in the store.

The input data for the numerical solution of the model are based on physical properties typical of stored grains and they are $C_f = 1.0048$ kJ/kgK, $C_m = 1.117$ kJ/kgK, $C_s = 1.3$ kJ/kgK, $C_w = 4.187$ kJ/kgK (Sutherland *et al.* 1971), $D_{eff} = 0.6175 \times 10^{-5}$ m²/s (Thorpe *et al.* 1991a,b), $\partial h_v/\partial T' = -2.3768$ kJ/kgK (derived from data presented by Keenan and Keyes 1936), $H = 5.0$ m, $K = 2.5159 \times 10^{-8}$ m² (derived from Hunter 1983), $L = 20.0$ m, $q_H = 15778$ kJ/kg (Thompson 1972), $q_w = 0.6$, $\Delta T' = 10C$, $\beta = 1/293.15$, $\kappa_{eff} = 1.64 \times 10^{-4}$ kW/mK (Chung and Lee 1986), $\rho_f = 1.2$ kg/m³, $\rho_s = 690.0$ kg/m³ (Sutherland *et al.* 1971) and $\mu = 18.1 \times 10^{-6}$ kg/ms (Dunkle and Ellul 1972). With respect to these input data, the numerical values of the Darcy-Rayleigh number is obtained by using Eq. (15) as 20.65.

For the purpose of selecting a suitable mesh size that yields accurate results, the effect of grid points on the numerical solution was tested by a series of runs of the program. The number of grid points employed in the numerical experiments is taken from 21 × 21 to 41 × 41 grid points. It was observed that a grid of 41 × 41 nodal points as shown in Fig. 1(b) results in convergence of the solution. By trial and error it is observed that the value 0.2 is suitable for the transient parameter, α_ψ in numerical experiments. In spite of the fact that the criterion $\psi_{err} = 10^{-4}$ requires approximately about 40% more iterations compared to $\psi_{err} = 10^{-3}$, the numerical experiments were performed by taking the previous criterion in order to ensure more accurate results during the early stages of our numerical calculations. As pointed out by Singh *et al.* (1993) free convective heat transfer in porous media contained in enclosures that have simple two-dimensional geometries has been well-investigated. They note that the mathematical modelling technique adopted in this paper yield results that compare well with established solutions.

RESULTS AND DISCUSSION

The use of the model is demonstrated by considering a cross section of a peaked bulk of maize stored between two vertical walls placed 20 m apart. The wall height of the grain is 5 m and the angle of response, γ, is taken to be 22.5°. The floor is deemed to be adiabatic and the entire system boundary is impermeable to moisture. The surfaces of bunkers are exposed to diurnal fluctuations in temperature as a result of changes in the ambient air temperature, solar radiation, thermal radiation to the sky and so on. However, for the sake of clarity in presenting the potential utility of the model the short term variations are neglected, and a step change in the surface temperature of the grain is imposed. This highlights the rate at which the grain cools and the mechanisms of the moisture migration.

The initial temperature of the grain is 30C, corresponding to a dimensionless value of 1.0 and the moisture content is 14% wet basis (16.28% dry basis). A temperature of 20C is imposed on the upper surface and the side walls and the resulting temperature distribution in the grain after 120 days storage is shown in Fig. 2. Values of the stream function are shown in Fig. 3. Each contour in the figure represents a streamline along which the air travels. The velocity field is readily obtained from the stream function. Qualitatively we expect the vertical component of the velocity to be greatest when the horizontal gradient of stream function is the greatest. In the case of the system studied here, this occurs close to the vertical walls. Examination of Fig. 3 prompts us to realize that the horizontal component of the velocity is likely to be greatest near the upper surface of the bulk and in the lower corners. Figures 4 and 5, which show the vertical and horizontal components of velocity, confirm the qualitative expectations.

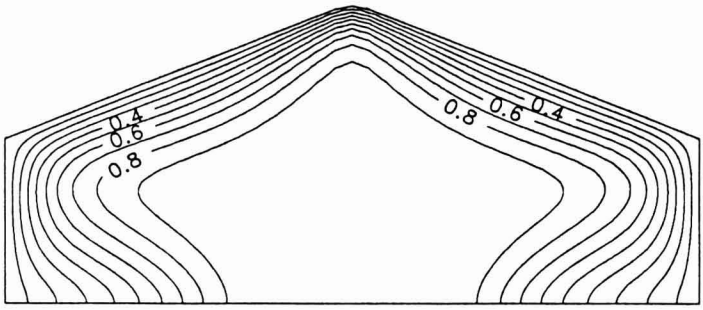

FIG. 2. TEMPERATURE DISTRIBUTION

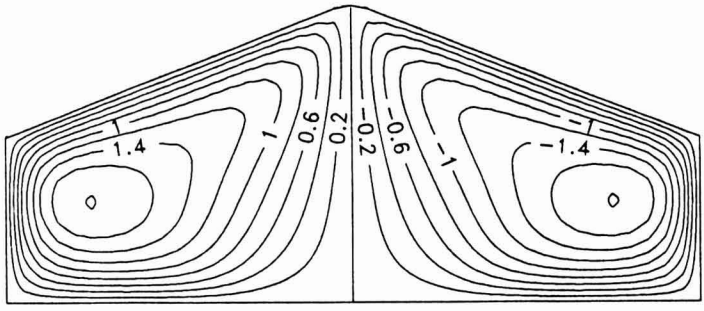

FIG. 3. VALUES OF THE STREAM FUNCTION

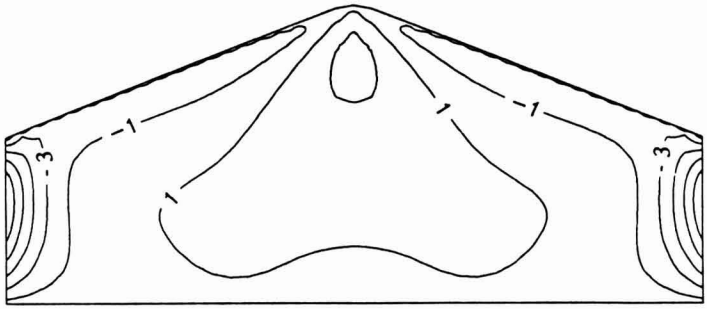

FIG. 4. VERTICAL COMPONENT OF THE VELOCITY

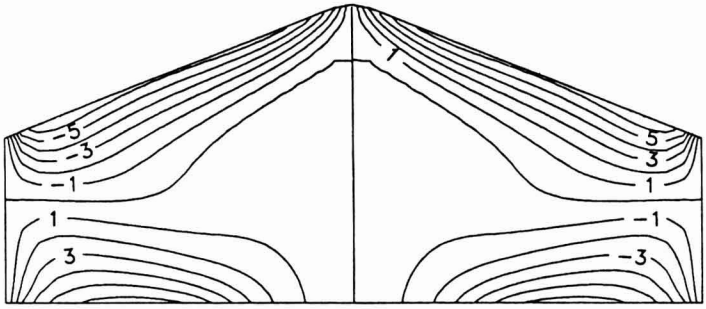

FIG. 5. HORIZONTAL COMPONENT OF THE VELOCITY

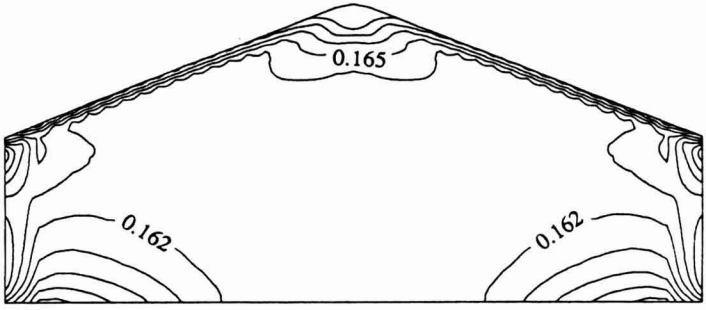

FIG. 6. MOISTURE CONTENT OF THE GRAIN

Figure 6 indicates how moisture is redistributed within the grain bulk. The moisture content of the grain increases near the peak as a result of warm air rising from the interior of the bulk. The warm air has a high absolute humidity and as it approaches the cool upper surface its relative humidity increases, and the grains in this region adsorb moisture.

The rate at which the grains lose dry matter is a function of temperature, grain moisture content and physiological time. It is clear from Fig. 7 that most dry matter is lost in the center of the bulk where the temperature is highest. The rate of pesticide decay, in this case fenitrothion, shows similar behavior, as illustrated by Fig. 8. Again, the most rapid rate of loss is in the center of the bulk where the temperature is the highest.

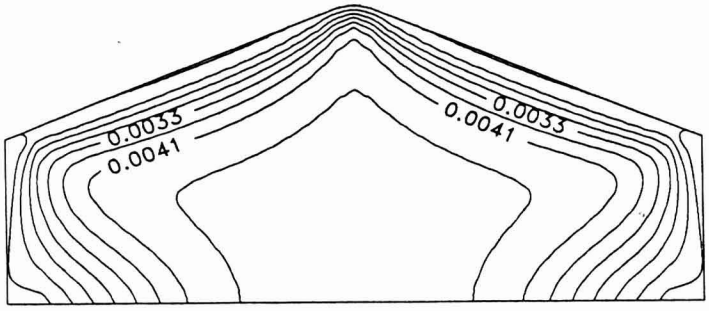

FIG. 7. DRY MATTER LOSS

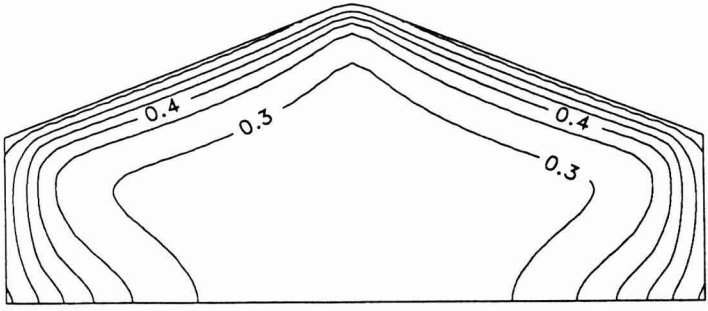

FIG. 8. PESTICIDE CONCENTRATION

CONCLUSIONS

An algebraic grid generation technique has been used to simulate heat and moisture transfer in grain bulks of arbitrary geometry. The solution methodology accommodates the problems where the boundaries of solution domain do not coincide with the coordinate lines. The theory has been used to model temperature, moisture content, velocity, pesticide concentration and dry matter loss in a bunker store containing maize.

ACKNOWLEDGMENT

The authors gratefully acknowledge the Wheat Research Council for providing financial support to carry out this work.

NOMENCLATURE

Arx	Ratio of width to wall height of bunker
B	Pesticide-specific empirical constant, C^{-1}
C_f	Specific heat of intergranular air at constant pressure, kJ/(kg dry air K)
C_i	Initial concentration of pesticide kg/m^3
C_m	Specific heat of dry grain, kJ/(kg dry grain K)
C_{pes}	Pesticide concentration, kg/m^3
C_s	Defined in Eq. (5), kJ/(kg dry grain K)
C_w	Specific heat of liquid water, kJ/(kg water K)
d_m	Dry matter loss, kg/kg
D_{eff}	Effective diffusivity of moisture vapor in the grain bulk, m^2/s
$f_1,\ldots,f_4$	Functions representing the boundaries of the grain store
g	Acceleration due to gravity, m/s^2
h_s	Latent heat of vaporization of water in grain, kJ/(kg water)
h_v	Latent heat of vaporization of pure water, kJ/(kg water)
H	Height of vertical walls, m
K	Permeability of packed bed, m^2
L	Distance between vertical walls, m
n	Unit outward normal vector
n_x, n_y	Direction cosines of outward normal of boundary $f_4(x, y) = 0$
p′	Pressure, Pa
q_H	Heat of oxidation, kJ/kg
q_w	Rate of moisture libration as a result of respiration, kg water/(kg dry matter)

Nomenclature (*cont.*)

r	Relative humidity of intergranular air
Ra	Darcy-Rayleigh number
t	Nondimensional time
t_d, t_i	Defined in Eq. (14)
t_{mx}, t_{my}	Defined in Eq. (28)
t_w	Defined in Eq. (14)
t′	Time, s
t*	Pesticide-specific empirical constant, s
T	Temperature in nondimensional form
T′	Temperature, C
T'_o	Ambient temperature, C
T'_g	Initial temperature of the stored grain, C
u, v	Nondimensional velocity components
u′, v′	Velocity components, m/s
V′	Velocity vector, m/s
w	Moisture content of intergranular air, kg water/(kg dry air)
w_d, w_i	Defined in Eq. (14)
W	Moisture content of grain, kg water/(kg dry grain)
x, y	Nondimensional coordinates
y′, y′	Coordinates, m

Greek symbols

$\alpha_1,\ldots,\alpha_4$	Defined in Eq. (28)
α_ψ	False transient term
β	Coefficient of thermal expansion, K^{-1}
$\beta_1,\ldots,\beta_5$	Defined in Eq. (28)
γ	Angle of repose of grain
$\Delta T'$	Temperature difference, C
∇'	Gradient operator, m^{-1}
∇'^2	Laplacian operator, m^{-2}
κ_{eff}	Effective conductivity of bulk stored grains, kW/mK
ρ_f	Density of intergranular air, kg/m³
ρ_{of}	Density of intergranular air at ambient temperature, kg/m³
ρ_s	Density of wet grain, kg/m³
μ	Viscosity of intergranular air, kg $m^{-1}s^{-1}$
ϕ	Any function of x and y
ψ	Nondimensional stream function
ψ_{err}	Error criterion for determining the approach to steady-state of the stream function
ψ'	Stream function, m²/s
ξ, η	Nondimensional transformed coordinates

REFERENCES

CHEN, J.C., SHEU, J.C. and JWU, S.S. 1990. Numerical computation of thermocapillary convection in a rectangular cavity. Numerical Heat Transfer *17A*, 287–308.

CHIU, C.P. and WU, T.S. 1990. Study of air motion in reciprocating engine using an algebraic grid generation technique. Numerical Heat Transfer *17A*, 309–327.

CHUNG, D.S. and LEE, C.-H. 1986. Physical and thermal properties of grains. In *Preserving Grain Quality by Aeration and In-Store Drying*. Proceedings of an International Seminar held in Kuala Lumpur, 9–11, Oct. 1985, ACIAR Proc. No. 15, pp. 53–66, Canberra, Australia.

DESMARCHELIER, J.M. and BENGSTON, M. 1979. Chemical residues of newer grain protectants. In *Australian contributions to the symposium on the protection of grain against insect damage during storage*, (D.E. Evans, ed.), pp. 108–115, Moscow 1978, CSIRO Division of Entomology, Canberra.

DE VAHL DAVIS, G. 1976. Program FRECON for the numerical solution of free convection in a rectangular cavity. Report 1976/FMT/1, School of Mechanical and Industrial Engineering, University of New South Wales, NSW, Australia-2033.

DOUGLAS, J. and RACHFORD, H.H. 1956. On the numerical solution of heat conduction problems in two and three space variables. Trans. Amer. Math. Soc. *3*, 421–439.

DUNKLE, R.V. and ELLUL, W.M.J. 1972. Randomly packed particulate bed regenerators and evaporative coolers. Trans. Mech. Eng. IEAust, MC8: 117–121.

FREER, M.W., SIEBENMORGEN, T.J., COUVILLION, R.J. and LOEWER, O.J. 1990. Modeling temperature and moisture content changes in bunker-stored rice. Trans. ASAE *33*, 211–220.

GRIFFITHS, H.J. 1964. Bulk storage of grain: A summary of factors governing control of deterioration. CSIRO Division of Mechanical Engineering, Report ED8, Highett, Victoria, Australia.

HUNTER, A.J. 1983. Pressure difference across an aerated seed-bulk for some common duct and store cross-sections. J. Agric. Eng. Res. *28*(5), 437–450.

HUNTER, A.J. 1987. An isostere equation for some common seeds. J. Agric. Eng. Res. *37*, 93–105.

KEENAN, J.H. and KEYES, F.G. 1936. *Thermodynamic Properties of Steam*, John Wiley & Sons, New York.

LEE, T.S. 1984. Computational and experimental studies of convective fluid motion and heat transfer in inclined non-rectangular enclosures. Int. J. Heat Fluid Flow *5*, 29–36.

MALLINSON, G. and DE VAHL DAVIS, G. 1973. The method of false tran-

sient for the solution of coupled elliptic equations. J. Comput. Phys. *12*, 435–461.

MORETTI, G. and ABBETT, M. 1966. A time-dependent computational method for blunt body flows. AIAAJ *4*, 2136–2141.

NGUYEN, T.V. 1987. Natural convection effects in stored grains: A simulation study. Drying Technol. *5*, 541–560.

PEACEMAN, D.W. and RACHFORD, H.H. 1955. The numerical solution of parabolic and elliptic differential equations. J. Soc. Ind. Appl. Math. *3*, 28–41.

SAITOH, T. 1978. Numerical method for multi-dimensional freezing problems in arbitrary domains. Trans. ASME J. Heat Transfer *100*, 294–299.

SHYY, W., TONG, S.S. and CORREA, S.M. 1985. Numerical recirculating flow calculation using a body-fitted coordinate system. Numerical Heat Transfer *8*, 99–113.

SINGH, A.K. and THORPE, G.R. 1993. Three-dimensional natural convection in a confined fluid overlying a porous layer. J. Heat Transfer. (In Press).

SUTHERLAND, J.W., BANKS, P.J. and GRIFFITHS, H.J. 1971. Equilibrium heat and moisture transfer in airflow through grain. J. Agric. Eng. Res. *16*(4), 368–386.

THOMPSON, T.L. 1972. Temporary storage of high-moisture shelled corn using continuous aeration. Trans. ASAE *15*, 333–337.

THORPE, G.R. 1986. Some fundamental principles and benefits of aeration of stored grains. In *Preserving Grain Quality by Aeration and In-Store Drying*, Proceeding of an International Seminar held in Kuala Lumpur, ACIAR Proc. No. 15, pp. 31–44, Canberra, Australia.

THORPE, G.R., MOORE, G.A. and SINGH, A.K. 1992. Heat, mass and momentum transfer in three-dimensional bulks of stored grains. Institution of Engineers Australia Conference on Engineering in Agriculture, pp. 91–96, Albury, Australia, 4–7 Oct. 1992.

THORPE, G.R. and NGUYEN, T.V. 1987. The response of non-ventilated grain to environmental temperature. In *Proceedings of 4th International Working Conference on Stored-Product Protection* (E. Donahaye and S. Navarro, eds.) pp. 230–242, Tel Aviv, Israel, Sep. 1986.

THORPE, G.R., OCHOA, J.A. and WHITAKER, S. 1991a. The diffusion of moisture in food grains. I. The development of a mass transfer equation. J. Stored Prod. Res. *27*, 1–9.

THORPE, G.R., OCHOA, J.A. and WHITAKER, S. 1991b. The diffusion of moisture in food grains. II. The development of constraints. J. Stored Prod. Res. *27*, 11–30.

YATES, C.J. and STICKA, R. 1984. Development and future trends in bunker storage. In *Controlled Atmosphere and Fumigation in Grain Storages*, (B.E. Ripp, ed.) pp. 589–600, Elsevier, New York. (Proc. Int. Symp. "Practical Aspects of Controlled Atmosphere and Fumigation in Grain Storages," Apr. 11–12, 1983, Perth, Australia).

DIVIDED SORPTION ISOTHERM CONCEPT: AN ALTERNATIVE WAY TO DESCRIBE SORPTION ISOTHERM DATA

M.G. ISSE,[1] H. SCHUCHMANN and H. SCHUBERT

Institute of Food Process Engineering
Karlsruhe University
Karlsruhe, Germany

Accepted for Publication October 27, 1992

ABSTRACT

The broad range of moisture sorption isotherm (MSI) data of mango is divided into two ranges of submoisture sorption isotherms (sub-MSI), corresponding to two different ranges of water activity; the net isosteric heat of sorption (q_{st}) is used as subdivision criterion of these two ranges. The sub-MSI are fitted to a general elquation. The mean error is 5% for the first sub-MSI (q_{st}) and 10% for the second ($q_{st} \leqslant 0$).

INTRODUCTION

The knowledge of moisture sorption isotherms (MSI) is important to predict microbiological, enzymatic and chemical stability, to select packing materials, to design drying and concentration processes as well as for storage of food.

Several equations have been proposed for the description of equilibrium moisture sorption isotherms (Chirife and Iglesias 1978); their applicability to different types of foods and throughout the entire water activity scale is limited, however. This is mainly because MSI of heterogeneous products such as food represent the integrated hygroscopic properties of the different constituents, which in most cases cannot be predicted. Each of these hygroscopic properties may be predominant in a given water activity range (Karel 1973). A better description of the sorption data in the entire water activity range could be realized through a formal division of MSI data into sub-MSI, corresponding to different ranges of water activity.

[1]Mailing address: Dipl.-Ing. M.G. Isse, Institut für Lebensmittelverfahrenstechnik, Universität Karlsruhe, Kaiserstraβe 12, 7500 Karlsruhe 1, Germany.

Journal of Food Process Engineering **16** (1993) 147–157.

A relation between the ranges of sub-MSI and the stability of foods is reported (Rockland 1969); however, no criterion to divide MSI into sub-MSI data is proposed.

In the present report the concept of sub-MSI is applied to mango moisture sorption data. Two sub-MSIs are considered and as subdivision criterion the net isosteric heat (q_{st}) is proposed. This property can be calculated by formal application of the Clausius-Clapeyron equation to the equilibrium data (Gál 1967), (Rizvi 1986),

$$q_{st} = -R\ d(\ln a_w)/d(a/T) \tag{1}$$

where q_{st} is defined as the total heat of sorption in the food minus the heat of vaporization of water at the system temperature, a_w is the water activity, R is the universal gas constant and T is the absolute temperature.

Equation (1) could be easily integrated, assuming that q_{st} does not depend significantly upon the temperature:

$$a_w = \text{const} \cdot \exp(-q_{st}/R \cdot T) \tag{2}$$

The q_{st} was chosen to divide the MSI, because this property provides information about the water binding capacity of foods, similarly to the water activity (Rizvi 1986); as a thermodynamic property it can be also applied to every food material. For sugar containing foods such as fruits, and particularly osmotically treated ones, the q_{st} changes sign (Saravacos *et al.* 1986), probably because of the heat of solution of the sugars in the food material; this fact simplifies the use of q_{st} as dividing criterion of the MSIs of sugar containing materials.

MATERIAL AND METHODS

Commercial mangoes (*Mangifera indica* L.), obtained from the Mogadishu market soon after harvest, were transported by plane to Karlsruhe and placed into a cold store (12C, 98% humidity). The mangoes were cut into cylindrical pieces of 3 mm thickness and weighted. Afterwards they were either dried in vacuum (70C for 24 h) immediately, or first treated with an osmotic 70% (w/w) sucrose solution (1 h at 50C) and vacuum-dried subsequently. The total solids content of mango with and without osmotic treatment is 27 + 1%, and 17 + 1% (g solids/g initial wet mango). Samples of mangoes with and without osmotic treatment were used to determine moisture sorption isotherms from 26 to 50C. The static equilibrium method, developed in the EEC COST 90 project (Spiess and Wolf 1983) was applied. Samples of about 400 mg dried mango each were

ground with a mortar and placed into ten hydrostats of constant relative humidity (RH). A constant RH was maintained by saturated salt solutions. For each sample and RH three replicates were made. Within seven days of moisture adsorption the equilibrium was reached.

RESULTS AND DISCUSSION

The adsorption isotherm data of mangoes (Fig. 1a, 1b) are not sigmoid and the temperature dependency varies with the water activity, crossing themselves at an a_w value above 0.5. This is in agreement with literature data for sugar containing foods (Saravacos *et al.* 1986).

Different equations proposed in the literature (Iglesias and Chirife 1982) were used to describe the adsorption data of mango. In order to calculate the goodness

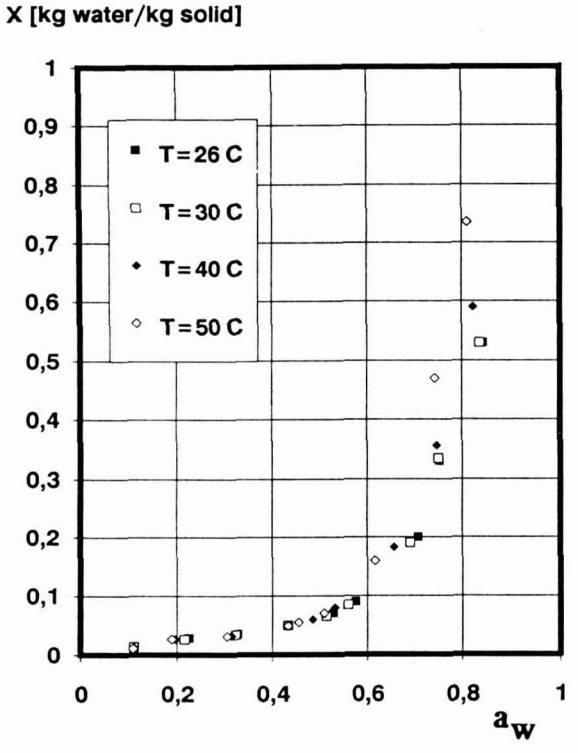

FIG. 1a. SORPTION ISOTHERMS OF MANGO (WITHOUT OSMOTIC TREATMENT) AT DIFFERENT TEMPERATURES

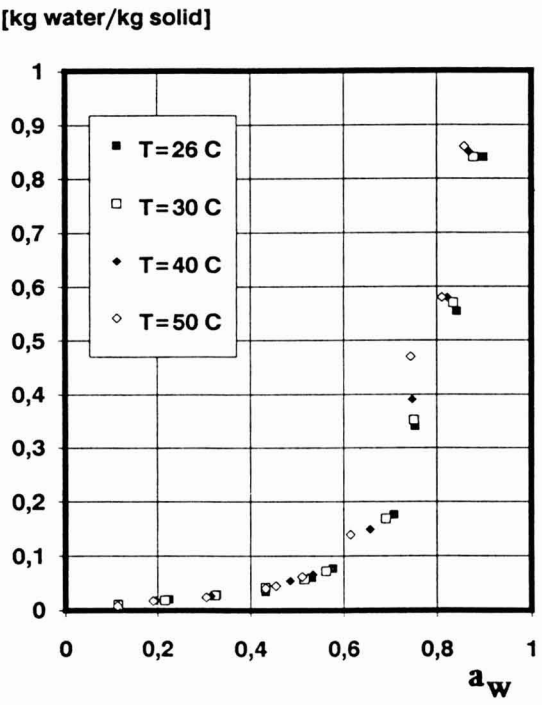

FIG. 1b. SORPTION ISOTHERMS OF OSMOTICALLY TREATED MANGO AT DIFFERENT TEMPERATURES

of fit of the various equations to the experimental data, a mean relative deviation (MRD) was adopted:

$$MRD = \frac{100}{n} \Sigma \frac{|X_{e,i} - X_{p,i}|}{Xe} \tag{3}$$

where Xe and Xp, respectively, are the experimental and predicted values of the water content and n is the number of the experimental data. Table (1) shows the MRD of adsorption isotherm data of mango (without osmotic treatment) at 26C fitted with different equations.

Other MSI data give similar MRD. Halsey's two parameter equation is the only one that gives an acceptable description of the entire MSI. In the case of divided moisture sorption isotherms, Henderson's equation gives the best description of the sub-MSI data.

Table 2 shows the calculated net isosteric heat of adsorption for mangoes at the given moisture contents with and without osmotic treatment (Eq. 2).

TABLE 1.
MEAN ERROR FOR DIFFERENT MOISTURE SORPTION ISOTHERM EQUATIONS, CALCULATED FROM MANGO DATA (26.5C) ACCORDING TO THE EQUATIONS GIVEN IN IGLESIAS AND CHIRIFE (1982)

Equation		MRD% MSI	MRD% sub-MSI
Gab	$X = \frac{C\ K\ a_w\ X_m}{(1 - K\ a_w)(1 - K\ a_w + C\ k\ a_w)}$	22	10.3
Bradley	$\ln 1/a_w = A\ B^X$	132	8.6
Halsey	$a_w = \exp(-A / X^B)$	9.5	7.3
Henderson	$1 - a_w = \exp(-A\ X^B)$	29	4.7
Iglesias + Chirife	$\ln(X+(X^2 + X_{0.5})^{0.5} = A\ a_w + B$	85	10.5
Kuhn	$X = A / a_w + B$	43	6.4
Oswin	$X = A\ (a_w / (1 - a_w))^B$	20	5.7
Smith	$X = A - B \ln(1-a_w)$	98	7.9
Schuchmann, Roy, Peleg	$1/X = C / y\ A - 1 / B$;		
	$y = a_w$	28	10.9
	$y = a_w / (1 - a_w)$	28	10.9
	$y = \ln(1 /(1 - a_w))$	27	13.3

Considering two sub-MSIs and adopting the q_{st} value as subdividing criterion of the ranges of the two sub-MSIs, one may use the following general equation to fit the experimental data:

$$\ln X = A * f(a_w) + B \quad (4)$$

where $f(a_w)$ is a function of the water activity, A and B are constants for a given temperature which can be determined through linear regression. Henderson's and Halsey's equations are particular cases of Eq. (4).

The first sub-MSI is in an a_w range where $q_{st} > 0$. The sub-MSI data were fitted to Eq. (4). Figure 2 shows the experimental and predicted values according to Eq. (4) for mango without osmotic treatment for 26.5C. The Henderson's equation was adopted, because of its smaller mean error shown in Table 2.

The predicted values of sub-MSI for mango (without osmotic treatment) for

TABLE 2.
CALCULATED NET ISOSTERIC HEAT OF MANGO

X	a_w	q_{st}^{x}	q_{st}^{xx}
kg H_2O / kg TS		kJ / kg H_2O	kJ / kg H_2O
0.020	0.174 ± 0.019	30.1 ± 2.5	24.7 ± 0.4
0.030	0.265 ± 0.016	18.4 ± 4.2	7.5 ± 2.5
0.052	0.451 ± 0.003	3.3 ± 0.8	1.7 ± 1.7

x mango without osmotic treatment.
xx mango with osmotic treatment.

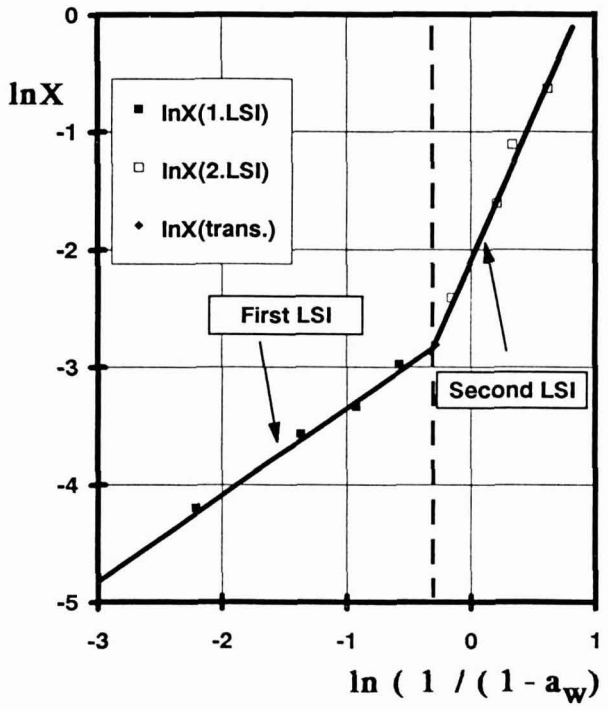

FIG. 2. EXPERIMENTAL AND PREDICTED VALUES ACCORDING TO EQ. (4) OF LSI FOR MANGO WITHOUT OSMOTIC TREATMENT AT 26C

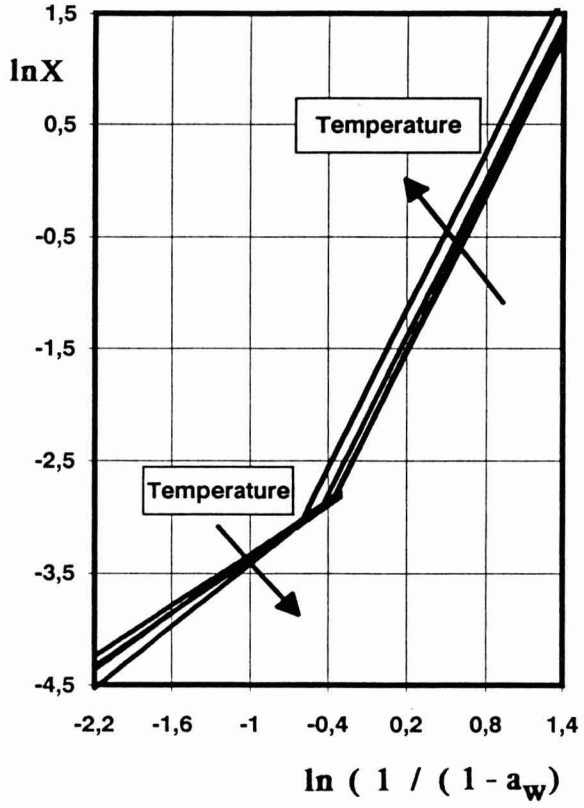

FIG. 3. PREDICTED LSI FOR MANGO (WITHOUT OSMOTIC TREATMENT) AT FOUR DIFFERENT TEMPERATURES

all temperatures are represented in Fig. 3. Analogous diagrams could be made for mango with osmotic treatment. Statistical analysis has shown that the slope of the Eq. (4a) for the first sub-MSI ($q_{st} > 0$) changes linearly with temperature (Fig. 4a), while for the intercept no significant dependence upon the temperature was observed.

For the second sub-MSI the slope has not been found to vary significantly with the temperature, while the intercept changes linearly with temperature (Fig. 4b). The values of the slope and intercept for the different conditions are shown in Table 3. Accordingly, the following equations may be used for the two sub-MSI:

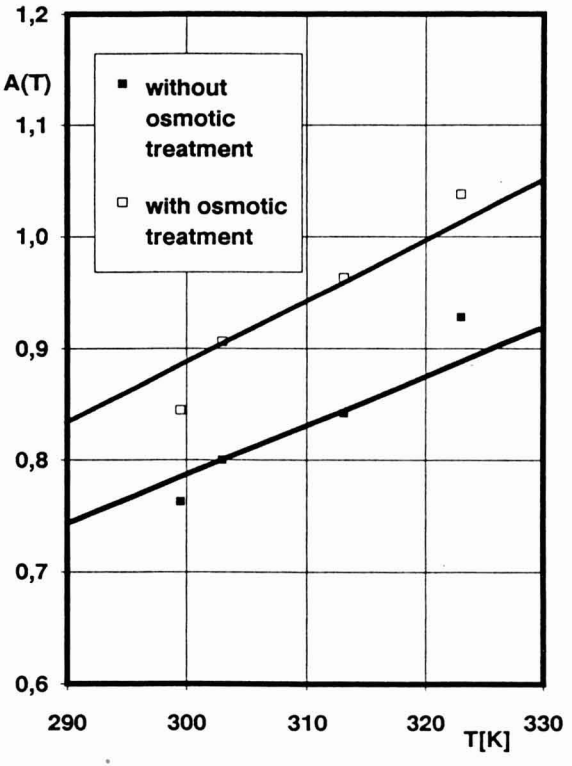

FIG. 4a. DEPENDENCE OF THE SLOPE I N EQ. (4a) UPON TEMPERATURE (FIRST LSI)

First sub-MSI ($q_{st} > 0$): $$\ln X = A(T) * f(a_w) + B \quad (4a)$$

Second sub-MSI ($q_{st} \leqslant 0$): $$\ln X = A * f(a_w) + B(T) \quad (4b)$$

with $f(a_w) = \ln(1/1-a_w))$ and A(T), B(T) being linear functions of the temperature, and X the water content (Kg_{H20}/Kg_{solid}). For a given temperature the a_w range corresponding to $q_{st} < 0$ is calculated from Eq. (1). Figure 5 shows a correlation between predicted and experimental values of the water content of mango (with and without osmotic treatment) for different temperatures. The MRD for the first and the second sub-MSI is 5% and 10%.

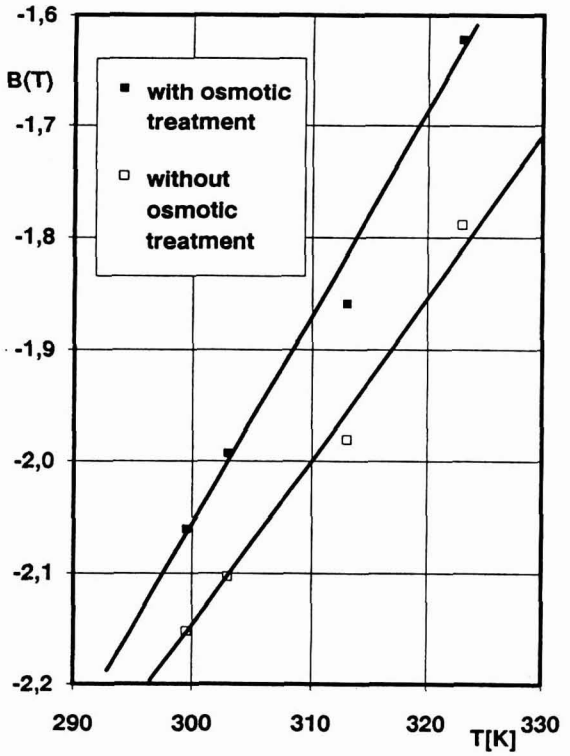

FIG. 4b. DEPENDENCE OF THE INTERCEPT IN EQ. (4b) UPON TEMPERATURE (SECOND LSI)

TABLE 3.
VALUES OF THE PARAMETERS IN EQ. (4a) AND (4b); THE TEMPERATURE IS IN °K

q_{st}	treatment	A	B
> 0	o.t.*	A(T) = 0.0078 T - 1.476	-2.676 + 0.041
> 0	n.t.*	A(T) = 0.0069 T - 1.289	-2.532 + 0.038
< 0	o.t.	-1.81 ± 0.10	B(T) = 0.014 T - 6.335
< 0	n.t.	-1.63 ± 0.08	B(T) = 0.019 T - 7.888

o.t. = mango with osmotic treatment
n.t. = mango without osmotic treatment

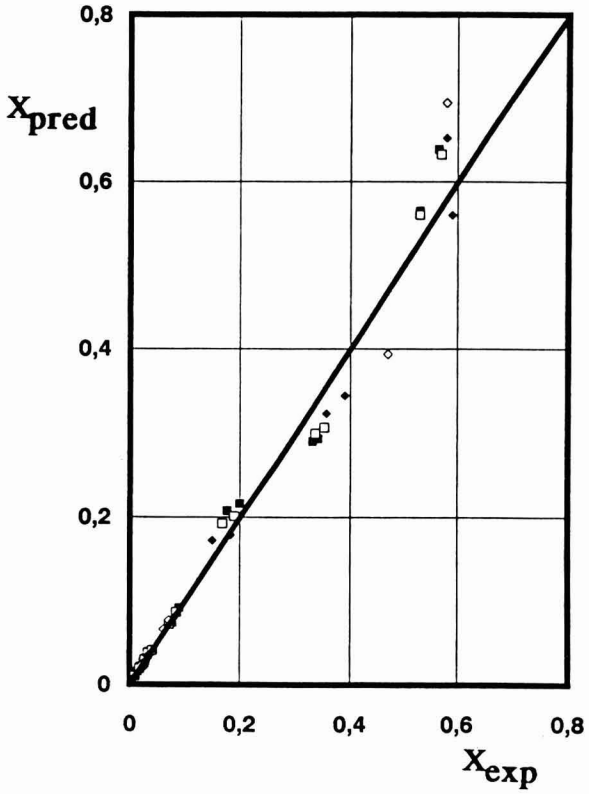

FIG. 5. CORRELATION BETWEEN PREDICTED AND EXPERIMENTAL VALUES OF WATER CONTENT FOR MANGO WITH AND WITHOUT OSMOTIC TREATMENT AT DIFFERENT TEMPERATURES

CONCLUSION

Throughout the whole range of the water activity the values obtained by the sub-MSI method have been found to fit the experimental data very well. The general equation is flexible and the constants could be easily determined through linear regression. The subdivision criterion of the sub-MSI is based on the isosteric heat value, which can be calculated by application of the Clausius-Clapeyron equation to the experimental data.

ACKNOWLEDGMENT

The authors thank the DAAD (German Academic Exchange Service) for support of their project.

REFERENCES

CHIRIFE, J. and IGLESIAS, H.A. 1978. Equations for fitting water sorption isotherms of foods: Part 1. A review. J. Food Technol. *30*, 159–174.

GÁL, S. 1967. *Die Methoden der Wasserdampf-Sorpionsmessungen*, p. 13, Springer Verlag, Berlin.

IGLESIAS, H.A. and CHIRIFE, J. 1982. *Handbook of Food Isotherms: Water Sorption Parameters for Food and Food Components*, pp. 262–265, Academic Press, New York.

KAREL, M. 1973. Recent research in the area of low moisture and intermediate moisture foods. Crit. Rev. Food Technol. *87*, 329–373.

RIZVI, S.S.H. 1986. Thermodynamic properties of foods in dehydration. In *Engineering Properties of Foods*, (M.A. Rao and S.S.H. Rizvi, eds.) pp. 133–214, Marcel Dekker, New York.

ROCKLAND, L.B. 1969. Water activity and storage stability. Food Technol. *23*, 11–21.

SARAVACOS, G.D., TSIOURVAS, D.A. and TSAMI, E. 1986. Effect of temperature on water adsorption isotherms of sultana raisins. J. Food Sci. *51*, 381–383.

SPIESS, W. and WOLF, W. 1983. The results of the COST-90 project on water activity. In *Physical Properties of Foods*, p. 65, Applied Science Publishers, London.

F N P PUBLICATIONS IN FOOD SCIENCE AND NUTRITION

Journals

JOURNAL OF FOOD LIPIDS, F. Shahidi
JOURNAL OF RAPID METHODS AND AUTOMATION IN MICROBIOLOGY, D.Y.C. Fung and M.C. Goldschmidt
JOURNAL OF MUSCLE FOODS, N.G. Marriott and G.J. Flick, Jr.
JOURNAL OF SENSORY STUDIES, M.C. Gacula, Jr.
JOURNAL OF FOODSERVICE SYSTEMS, C.A. Sawyer
JOURNAL OF FOOD BIOCHEMISTRY, J.R. Whitaker, N.F. Haard and H. Swaisgood
JOURNAL OF FOOD PROCESS ENGINEERING, D.R. Heldman and R.P. Singh
JOURNAL OF FOOD PROCESSING AND PRESERVATION, D.B. Lund
JOURNAL OF FOOD QUALITY, J.J. Powers
JOURNAL OF FOOD SAFETY, T.J. Montville and A.J. Miller
JOURNAL OF TEXTURE STUDIES, M.C. Bourne and P. Sherman

Books

FOOD CONCEPTS AND PRODUCTS, H.R. Moskowitz
MICROWAVE FOODS: NEW PRODUCT DEVELOPMENT, R.V. Decareau
DESIGN AND ANALYSIS OF SENSORY OPTIMIZATION, M.C. Gacula, Jr.
NUTRIENT ADDITIONS TO FOOD, J.C. Bauernfeind and P.A. Lachance
NITRITE-CURED MEAT, R.G. Cassens
THE POTENTIAL FOR NUTRITIONAL MODULATION OF THE AGING PROCESSES, D.K. Ingram *et al.*
CONTROLLED/MODIFIED ATMOSPHERE/VACUUM PACKAGING OF FOODS, A.L. Brody
NUTRITIONAL STATUS ASSESSMENT OF THE INDIVIDUAL, G.E. Livingston
QUALITY ASSURANCE OF FOODS, J.E. Stauffer
THE SCIENCE OF MEAT AND MEAT PRODUCTS, 3RD ED., J.F. Price and B.S. Schweigert
HANDBOOK OF FOOD COLORANT PATENTS, F.J. Francis
ROLE OF CHEMISTRY IN THE QUALITY OF PROCESSED FOODS, O.R. Fennema, W.H. Chang and C.Y. Lii
NEW DIRECTIONS FOR PRODUCT TESTING AND SENSORY ANALYSIS OF FOODS, H.R. Moskowitz
PRODUCT TESTING AND SENSORY EVALUATION OF FOODS, H.R. Moskowitz
ENVIRONMENTAL ASPECTS OF CANCER: ROLE OF MACRO AND MICRO COMPONENTS OF FOODS, E.L. Wynder *et al.*
FOOD PRODUCT DEVELOPMENT IN IMPLEMENTING DIETARY GUIDELINES, G.E. Livingston, R.J. Moshy, and C.M. Chang
SHELF-LIFE DATING OF FOODS, T.P. Labuza
ANTINUTRIENTS AND NATURAL TOXICANTS IN FOOD, R.L. Ory
UTILIZATION OF PROTEIN RESOURCES, D.W. Stanley *et al.*
VITAMIN B_6: METABOLISM AND ROLE IN GROWTH, G.P. Tryfiates
POSTHARVEST BIOLOGY AND BIOTECHNOLOGY, H.O. Hultin and M. Milner

Newsletters

FOOD INVESTMENT REPORT, G.C. Melson
MICROWAVES AND FOOD, R.V. Decareau
FOOD INDUSTRY REPORT, G.C. Melson
FOOD, NUTRITION AND HEALTH, P.A. Lachance and M.C. Fisher
FOOD PACKAGING AND LABELING, S. Sacharow

GUIDE FOR AUTHORS

Typewritten manuscripts in triplicate should be submitted to the editorial office. The typing should be double-spaced throughout with one-inch margins on all sides.

Page one should contain: the title, which should be concise and informative; the complete name(s) of the author(s); affiliation of the author(s); a running title of 40 characters or less; and the name and mail address to whom correspondence should be sent.

Page two should contain an abstract of not more than 150 words. This abstract should be intelligible by itself.

The main text should begin on page three and will ordinarily have the following arrangement:

Introduction: This should be brief and state the reason for the work in relation to the field. It should indicate what new contribution is made by the work described.

Materials and Methods: Enough information should be provided to allow other investigators to repeat the work. Avoid repeating the details of procedures which have already been published elsewhere.

Results: The results should be presented as concisely as possible. Do not use tables *and* figures for presentation of the same data.

Discussion: The discussion section should be used for the interpretation of results. The results should not be repeated.

In some cases it might be desirable to combine results and discussion sections.

References: References should be given in the text by the surname of the authors and the year. *Et al.* should be used in the text when there are more than two authors. All authors should be given in the Reference section. In the Reference section the references should be listed alphabetically. See below for style to be used.

DEWALD, B., DULANEY, J.T., and TOUSTER, O. 1974. Solubilization and polyacrylamide gel electrophoresis of membrane enzymes with detergents. In *Methods in Enzymology*, Vol. xxxii, (S. Fleischer and L. Packer, eds.) pp. 82–91, Academic Press, New York.

HASSON, E.P. and LATIES, G.G. 1976. Separation and characterization of potato lipid acylhydrolases. Plant Physiol. *57*,142–147.

ZABORSKY, O. 1973. *Immobilized Enzymes*, pp. 28–46, CRC Press, Cleveland, Ohio.

Journal abbreviations should follow those used in *Chemical Abstracts*. Responsibility for the accuracy of citations rests entirely with the author(s). References to papers in press should indicate the name of the journal and should only be used for papers that have been accepted for publication. Submitted papers should be referred to by such terms as "unpublished observations" or "private communication." However, these last should be used only when absolutely necessary.

Tables should be numbered consecutively with Arabic numerals. The title of the table should appear as below:

Table 1. Activity of potato acyl-hydrolases on neutral lipids, galactolipids, and phospholipids

Description of experimental work or explanation of symbols should go below the table proper. Type tables neatly and correctly as tables are considered art and are not typeset. Single-space tables.

Figures should be listed in order in the text using Arabic numbers. Figure legends should be typed on a separate page. Figures and tables should be intelligible without reference to the text. Authors should indicate where the tables and figures should be placed in the text. Photographs must be supplied as glossy black and white prints. Line diagrams should be drawn with black waterproof ink on white paper or board. The lettering should be of such a size that it is easily legible after reduction. Each diagram and photograph should be clearly labeled on the reverse side with the name(s) of author(s), and title of paper. When not obvious, each photograph and diagram should be labeled on the back to show the top of the photograph or diagram.

Acknowledgments: Acknowledgments should be listed on a separate page.

Short notes will be published where the information is deemed sufficiently important to warrant rapid publication. The format for short papers may be similar to that for regular papers but more concisely written. Short notes may be of a less general nature and written principally for specialists in the particular area with which the manuscript is dealing. Manuscripts which do not meet the requirement of importance and necessity for rapid publication will, after notification of the author(s), be treated as regular papers. Regular papers may be very short.

Standard nomenclature as used in the engineering literature should be followed. Avoid laboratory jargon. If abbreviations or trade names are used, define the material or compound the first time that it is mentioned.

EDITORIAL OFFICES: DR. D.R. HELDMAN, COEDITOR, *Journal of Food Process Engineering*, Food Science/Engineering Unit, University of Missouri-Columbia, 235 Agricultural/Engineering Bldg., Columbia, MO 65211 USA; or DR. R.P. SINGH, COEDITOR, *Journal of Food Process Engineering*, University of California, Davis, Department of Agricultural Engineering, Davis, CA 95616 USA.

CONTENTS